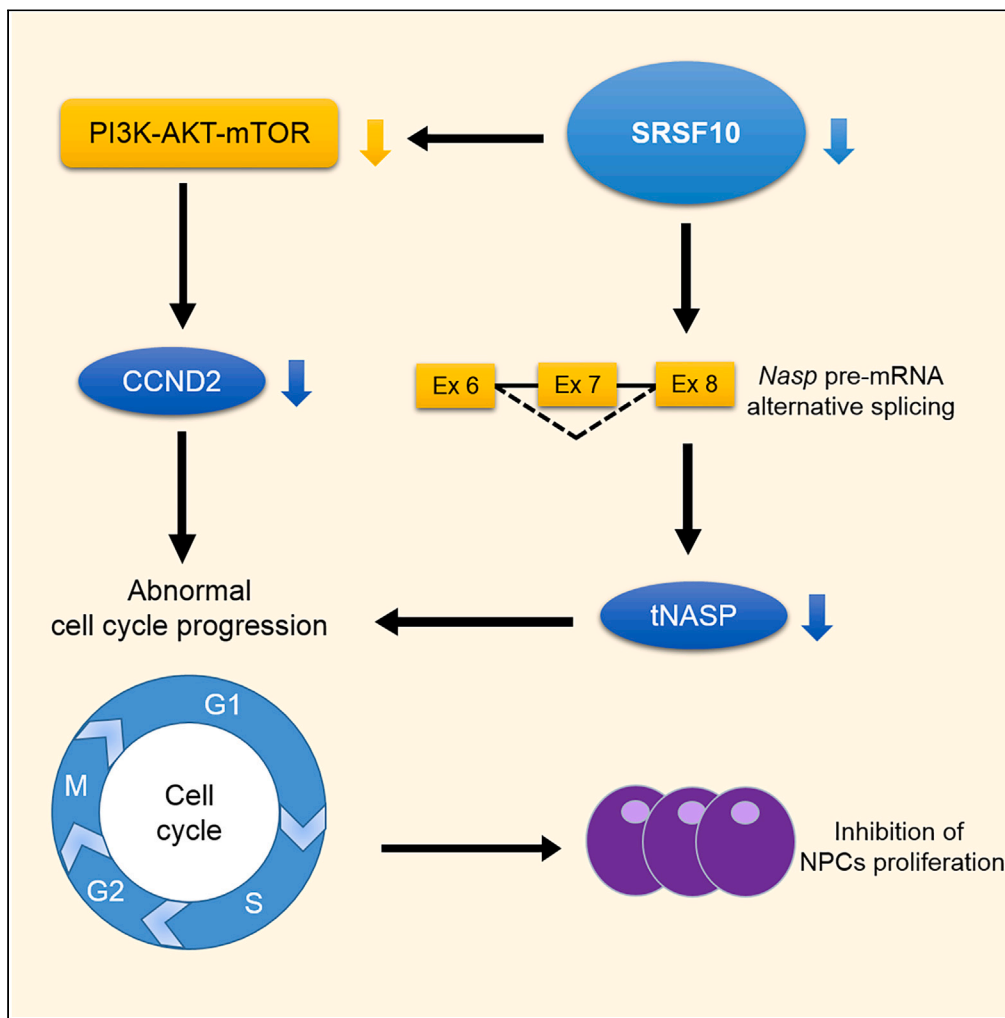


Article

SRSF10 regulates proliferation of neural progenitor cells and affects neurogenesis in developing mouse neocortex



Junjie Li, Hanyang Jiang, Yawei Mu, ..., Jingjing Zhao, Cuiqing Zhu, Xianhua Chen

xhchen@fudan.edu.cn

Highlights

SRSF10 knockout in NPCs causes dilated ventricle and thinned cortex in mouse brain

Dysfunction of SRSF10 inhibits NPCs proliferation and causes cell cycle abnormal

SRSF10 knockdown inhibits PI3K-AKT-mTOR-CCND2-signaling pathway in NPCs

SRSF10 knockdown alters the alternative splicing of *Nasp* exon 7 in NPCs



## Article

## SRSF10 regulates proliferation of neural progenitor cells and affects neurogenesis in developing mouse neocortex

Junjie Li,<sup>1,3</sup> Hanyang Jiang,<sup>1,3</sup> Yawei Mu,<sup>1,3</sup> Zixuan Wei,<sup>1</sup> Ankangzhi Ma,<sup>1</sup> Menghan Sun,<sup>1</sup> Jingjing Zhao,<sup>2</sup> Cuiqing Zhu,<sup>1</sup> and Xianhua Chen<sup>1,4,\*</sup>

## SUMMARY

**Alternative pre-mRNA splicing plays critical roles in brain development. SRSF10 is a splicing factor highly expressed in central nervous system and plays important roles in maintaining normal brain functions. However, its role in neural development is unclear. In this study, by conditional depleting SRSF10 in neural progenitor cells (NPCs) *in vivo* and *in vitro*, we found that dysfunction of SRSF10 leads to developmental defects of the brain, which manifest as abnormal ventricle enlargement and cortical thinning anatomically, as well as decreased NPCs proliferation and weakened cortical neurogenesis histologically. Furthermore, we proved that the function of SRSF10 on NPCs proliferation involved the regulation of PI3K-AKT-mTOR-CCND2 pathway and the alternative splicing of *Nasp*, a gene encoding isoforms of cell cycle regulators. These findings highlight the necessity of SRSF10 in the formation of a structurally and functionally normal brain.**

## INTRODUCTION

Proliferation of neural progenitor cells (NPCs) and neurogenesis are two critical processes in the early cortical development. The cerebral cortex is a finely layered structure of six layers and mediates multiple advanced functions including cognition and emotions.<sup>1,2</sup> Cortical neurons, including excitatory neurons and inhibitory interneurons, are all originated from NPCs. In short, neuroepithelial cells (NECs) undergo self-amplification and transition into radial glial cells (RGCs) that express PAX6.<sup>3</sup> RGCs, located in the ventricle zone (VZ), expand themselves through symmetrically division and generate intermediate progenitor cells (IPCs) through asymmetrically division.<sup>2,4</sup> IPCs, located in the subventricular zone (SVZ) and expressing the transcription factor TBR2, amplify themselves and produce neurons through symmetrically division.<sup>5,6</sup> While excitatory cortical projection neurons originate from the dorsal germinal regions of the telencephalon, inhibitory interneurons originate from the medial ganglionic eminence (MGE), and caudal ganglionic eminence (CGE).<sup>7</sup>

The proliferation and differentiation of NPCs involve a variety of regulation processes of gene expression. Among them, alternative pre-mRNA splicing (APS), as an important mechanism of transcriptome and proteome diversity, plays a critical role in regulating the development of NPCs. Dysregulation of APS can lead to abnormal development of NPCs and eventually lead to malformation of cerebrum.<sup>8–10</sup> However, the regulation mechanisms underlying these APS are largely unknown. Therefore, investigating how the alternative splicing of diverse transcripts is regulated during the NPCs development is of critical necessity for revealing the mechanism of cerebral developmental.

SR proteins (serine/arginine-rich proteins) are a family of RNA-binding proteins that can participate in tissue development as well as cell proliferation by regulating APS of genes.<sup>11–13</sup> SRSF10 (also nominated NSSR1), a member of SR protein family that is highly expressed in the nervous system, is implicated in the regulation of neuronal differentiation of P19 cells<sup>14</sup> and in *Xenopus laevis* as well.<sup>15</sup> It also plays a protective role in mouse brain by reducing neuronal injury after transient global cerebral ischemia.<sup>16</sup> The APS of a variety of neural functional genes have been reported to be regulated by SRSF10, such as NCAM-L1,<sup>14</sup> CREB,<sup>16,17</sup> SMN2,<sup>18</sup> and GluR-B,<sup>19</sup> which produce mRNA variants encoding protein isoforms of different functions in neural development.

<sup>1</sup>State Key Laboratory of Medical Neurobiology and MOE Frontiers Center for Brain Science, Institutes of Brain Science, Fudan University, Shanghai, China

<sup>2</sup>Center of Clinical Research, The Affiliated Wuxi People's Hospital of Nanjing Medical University, Wuxi 214023, PR China

<sup>3</sup>The authors contributed equally

<sup>4</sup>Lead contact

\*Correspondence: [xhchen@fudan.edu.cn](mailto:xhchen@fudan.edu.cn)

<https://doi.org/10.1016/j.isci.2023.107042>



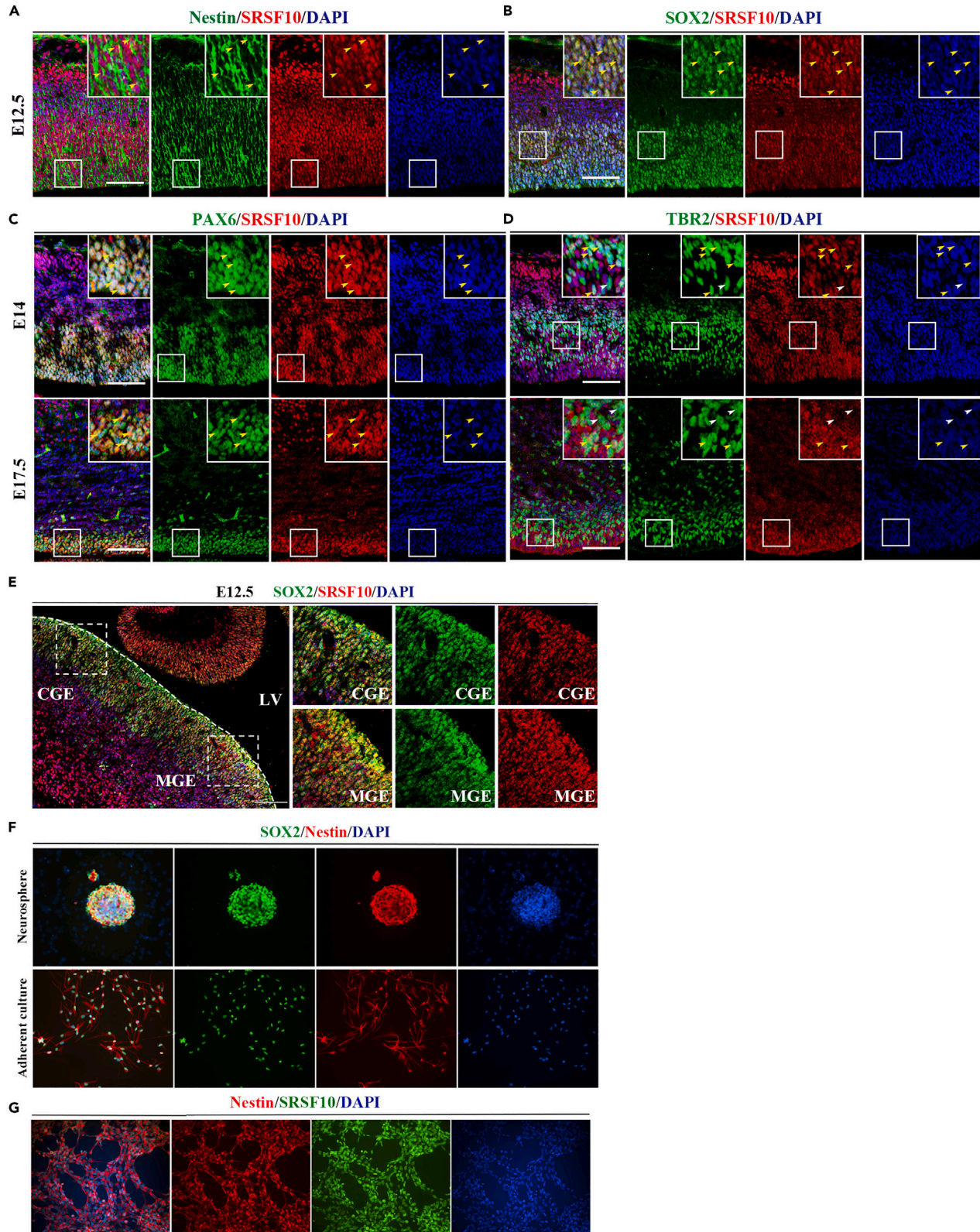


**Figure 1. SRSF10 is expressed in NPCs in the developing mouse neocortex, medial and caudal ganglionic eminences, and the primary NPCs**

(A–D) Double immunostaining images of SRSF10 and the NPCs markers Nestin (A), SOX2 (B), PAX6 (C), and TBR2 (D) in the cortex of embryonic mice at different developmental stages. E12.5 (A, B), E14, and E17.5 (C, D) mice were analyzed. The TBR2/SRSF10 double-positive cells (D) were highlighted by yellow arrows in the boxes, few cells were TBR2 positive while SRSF10 negative (highlighted by the white arrows).

(E) Double immunostaining images of SOX2 and SRSF10 in the CGE and MGE of E12.5 mice. MGE, Medial ganglionic eminences; CGE, Caudal ganglionic eminences.

(F–G) SRSF10 is expressed in primary NPCs. Double immunostaining of SOX2 and Nestin confirming the purity of primary NPCs in the neurosphere (upper panel in F) and in the adherent culture (lower panel in F), and double immunostaining images of Nestin and SRSF10 showing the expression of SRSF10 in primary NPCs (G). DAPI was used for counterstaining of nucleus. Scale bars represent 50  $\mu\text{m}$  for A–D, and 25  $\mu\text{m}$  for E and G. For analysis of brain sections, at least 3 mouse brains for each developmental stage were analyzed. For analysis of cultured NPCs, at least 3 batches of independent cultured NPCs were analyzed.

SRSF10 is also reported to play roles in multiple types of cancers,<sup>20–22</sup> including the glioblastoma (GBM), one of the most aggressive and lethal cancers of the brain which originates from neural stem or neural progenitor cells (NSCs/NPCs).<sup>23,24</sup> From the GEPIA database <http://gepia.cancer-pku.cn/detail.php?gene=SRSF10>, human GBM cells display a significantly altered mRNA expression level of SRSF10 compared with the normal cells, and the survival duration of the patients is negatively correlated with the expression level of SRSF10 in the GBM cells. Concerning the common neuroepithelial origins of GBM and NPCs,<sup>23,24</sup> and the high expression level of *Srsf10* RNA in the VZ region of mouse neocortex<sup>25</sup> which suggests that the SRSF10 protein may express in NPCs, we deduced that SRSF10 probably functions in NPCs development and neocortical neurogenesis. Besides, the participation of SRSF10 in the regulation of APS in mitosis<sup>26,27</sup> suggests that it may play important roles in NPCs proliferation. However, the specific roles of SRSF10 in early cerebral development, particularly in NPCs development, have not been revealed so far.

Here, by conditional inactivation of SRSF10 in the NPCs, we found that dysfunction of SRSF10 lead to developmental defects of the brain, which manifested as abnormal ventricle enlargement and cortical thinning of the context anatomically, as well as decreased NPCs proliferation and weakened cortical neurogenesis histologically. Furthermore, we proved that the function of SRSF10 on proliferation of NPCs involved its regulation of the PI3K-AKT-mTOR-CCND2 pathway and the alternative splicing of *Nasp*, a gene encoding isoforms of cell cycle regulation proteins. These findings highlight the necessity of SRSF10 expression in the formation of a structurally and functionally normal brain and may provide new insights into NPCs proliferation and cerebral developmental defects.

## RESULTS

### SRSF10 is expressed in NPCs *in vivo* and *in vitro*

In order to start with the investigation of the function of SRSF10 in the NPCs during mouse cerebral development, we analyzed the expression pattern of SRSF10 in NPCs in the brain samples of E12.5 mice using immunostaining. The results showed that SRSF10 protein was expressed in almost all the Nestin positive cells as well as SOX2 positive cells in neocortex (Figures 1A and 1B), and SOX2 positive cells in LGE, CGE, and MGE (Figure 1E). In addition, at E14 and E17.5, SRSF10 was also expressed in almost all PAX6 positive cells and TBR2 positive cells in the neocortex (Figures 1C and 1D).

We further investigated whether SRSF10 is expressed in NPCs *in vitro*. Primary NPCs were isolated from embryonic mouse neocortex, and the immunostaining results showed that SRSF10 protein was expressed in all the primary NPCs, which was confirmed by immunostaining positive for both SOX2 and Nestin (Figures 1F and 1G). Taken together, the ubiquitous expression of SRSF10 in NPCs during mouse cerebral development suggests that they might be important for NPCs function and neurogenesis.

### SRSF10 cKO mice display developmental defects with dilated ventricle and thinned cortex

To identify the potential functions of SRSF10 in NPCs and cerebral development, we constructed *Srsf10*<sup>fl<sub>ox</sub>/fl<sub>ox</sub></sup> mice, and conditionally deleted the exon 3 of *Srsf10* and knock out the SRSF10 protein in the NPCs by breeding with Nestin-Cre mice (Figures S1A–S1D). Immunostaining results showed that in SRSF10 heterozygous conditional knockout (HET cKO, *Srsf10*<sup>fl<sub>ox</sub>/+</sup> Nestin-Cre<sup>+</sup>) mice, the expression of SRSF10 protein in the brain was not significantly different from that in the *Srsf10*<sup>fl<sub>ox</sub>/fl<sub>ox</sub></sup> control mice (Ctrl, Figure S1E); whereas in SRSF10 conditional knockout (*Srsf10*<sup>fl<sub>ox</sub>/fl<sub>ox</sub></sup> Nestin-Cre<sup>+</sup>, SRSF10 cKO) mice, the expression of SRSF10 protein in the cortex and hippocampus was decreased significantly, as indicated by Western blot analysis (Figure S1D), and rarely detectable in neocortex by immunostaining (Figures S1F and S1G).

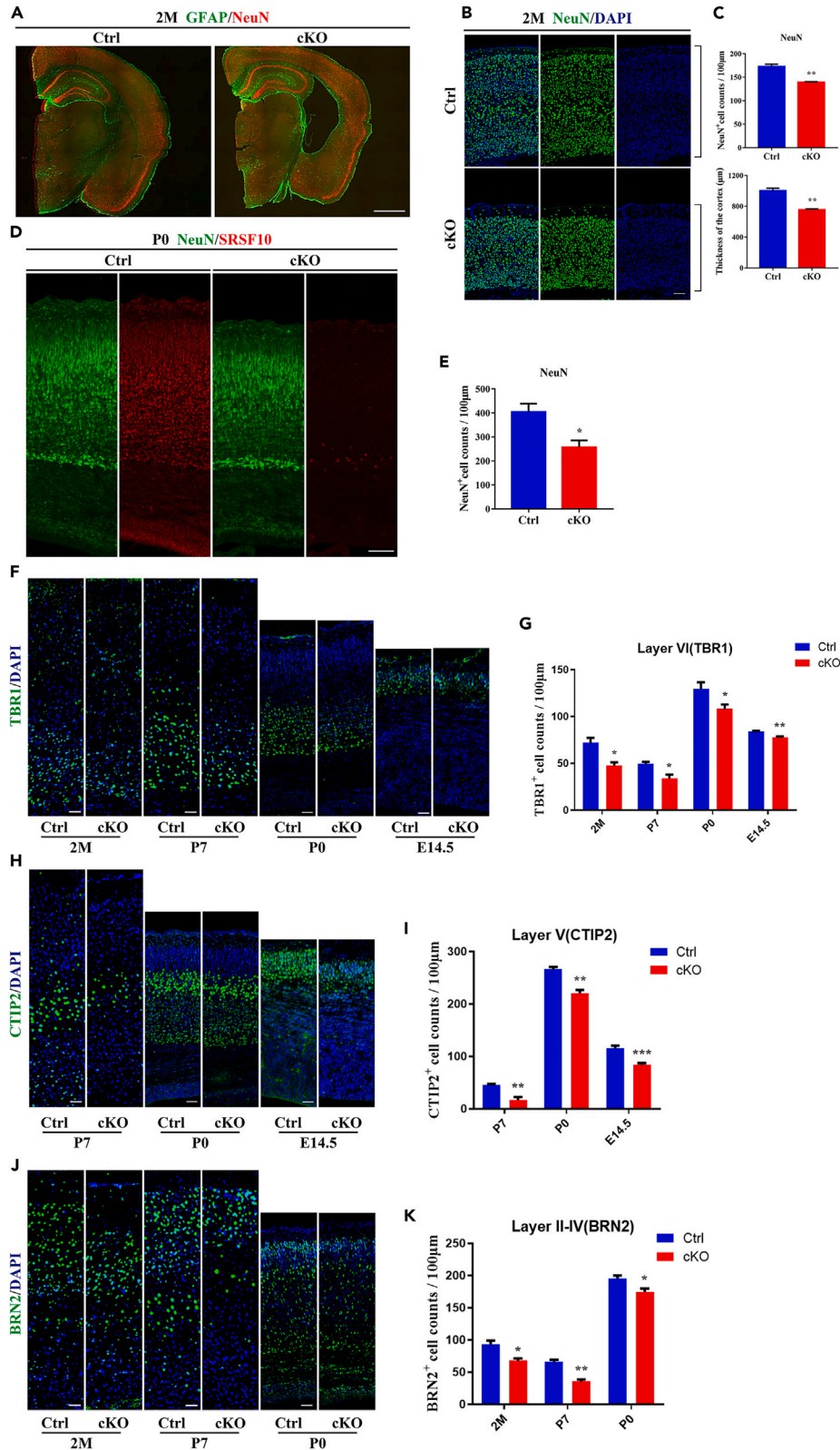


**Figure 2. SRSF10 cKO mice display developmental defects, with dilated ventricle and thinned cortex**

(A) Immunostaining images of astrocyte marker GFAP and mature neuron marker NeuN of the brain in the 2-month-old (2M) SRSF10 cKO (cKO) and control (Ctrl) mice. The *Srsf10*<sup>fl<sup>ox</sup>/fl<sup>ox</sup></sup> mice were used as the control of SRSF10 cKO mice. The dilated ventricle and the thinner cortex are remarkable. Scale bar represents 1000  $\mu$ m.

(B) Immunostaining images of NeuN in the cortex of 2M SRSF10 cKO mice. The thickness of the cortex was indicated and determined by the black lines on the right. Scale bar represents 100  $\mu$ m.

(C) The statistical data of B, showing the thickness of the cortex and the number of NeuN positive cells.

(D) Immunostaining images of NeuN and SRSF10 in the P0 mouse cortex, showing the expression of SRSF10 in the cKO mice is almost deleted. Scale bar represents 50  $\mu$ m.

(E) The statistical data of D, showing that the number of NeuN positive cells also decreased in the P0 SRSF10 cKO cortex, compared with the control.

(F, H, and J) Immunostainings images of the laminated neuronal markers TBR1 (F, layer VI), CTIP2 (H, Layer V), and BRN2 (J, Layer II to IV) in the cKO and control mouse cortex at E14.5, P0, P7, and 2M. (G, I, K) Statistical data of F, H, and J, respectively. Scale bars represent 25  $\mu$ m. Data are represented as mean  $\pm$  SEM. At least 3 mouse brains for each genotype were analyzed. For each mouse brain, at least 3 sections were counted. Student's t test for two-tailed distribution was used for comparison of two group of samples. \* $p < 0.05$ , \*\* $p < 0.01$ , \*\*\* $p < 0.001$ .

Then we investigated the effect of SRSF10 conditional knockout on mouse brain development. By immunostaining, we observed significantly dilated ventricle (ventriculomegaly) and significantly thinned cortex in the 2-month-old (2M) SRSF10 cKO mice, compared with those of non-cKO controls (Figures 2A and 2B). The number of mature neurons decreased significantly in the cortex of 2M cKO and P0 cKO mice, as indicated by NeuN staining (Figures 2B–2E). The reduced cortical thickness and neuronal number suggest that knockout of SRSF10 in NPCs causes development defect of mouse neocortex.

During brain development, a six-layer cortex structure generates from the NPCs in an “inside-out” manner, in which early born neurons occupy the deep layers of the neocortex, while later-born neurons migrate past these neurons.<sup>28</sup> To further investigate whether knockout of SRSF10 affects cortical neurogenesis of different layers, the brain sections of mice from 2M to E14.5 were immunostained using layer-specific neuronal markers (TBR1 for layer VI; CTIP2 for layer V; and BRN2 for layer II–IV). The results showed that the numbers of all of the TBR1-positive neurons, CTIP2-positive neurons, and BRN2-positive neurons decreased significantly in the SRSF10 cKO mice cortex at E14.5, P0, P7, and 2M (Figures 2F–2K), compared with those in the corresponding control mice. These results indicate that SRSF10 deletion leads to decreased number of neurons in each layer of the cortex, from the development stage at least as early as E14.5.

**SRSF10 knockout in NPCs results in impaired learning and memory ability and increased anxiety for adult mice**

The significant decreases in the thickness and neuronal number of cortex in SRSF10 cKO mice suggest that the function of the cerebral cortex may be impaired. We then performed behavioral tests to assess whether SRSF10 knockout affects the behavior of adult mice. Y-maze test was used to evaluate spontaneous alternation as a measure of working memory. The results showed that the cKO mice showed significant reductions in all the parameters including the number of alternations, max alterations, as well as the alteration behavior (Figure 3A). Rotarod test was used to evaluate motor coordination after repeated learning; the results showed that the latency to fall from the rotating rotarod for cKO mice was significantly decreased from the second day of learning, indicating the decreased ability in the coordinated movements after repeated learning (Figure 3B). These results indicate that SRSF10 knockout resulted in impaired learning and memory ability of mice. In the open-field test, the residence time in the central area was shortened, and the number of times of entering the central area was reduced for the cKO mice, while the total distance of movement between the cKO and the control mice showed no difference (Figures 3C and 3D), suggesting that the anxiety was increased in the cKO mice compared with the control mice. However, in the elevated plus-maze test, the cKO mice showed a trend to spend more time in the open arms (Figure 3E), implying that the risk prediction ability may be decreased. In the tail suspension test and forced swimming test, there was no significant difference in the duration of giving up struggling between the cKO and the control mice (Figures 3F and 3G), suggesting no alteration in despair or depression emotion in the cKO mice. Taken together, the above results show that knocking out of SRSF10 in NPCs attenuates the ability of mice in learning and memory and increased their anxiety.

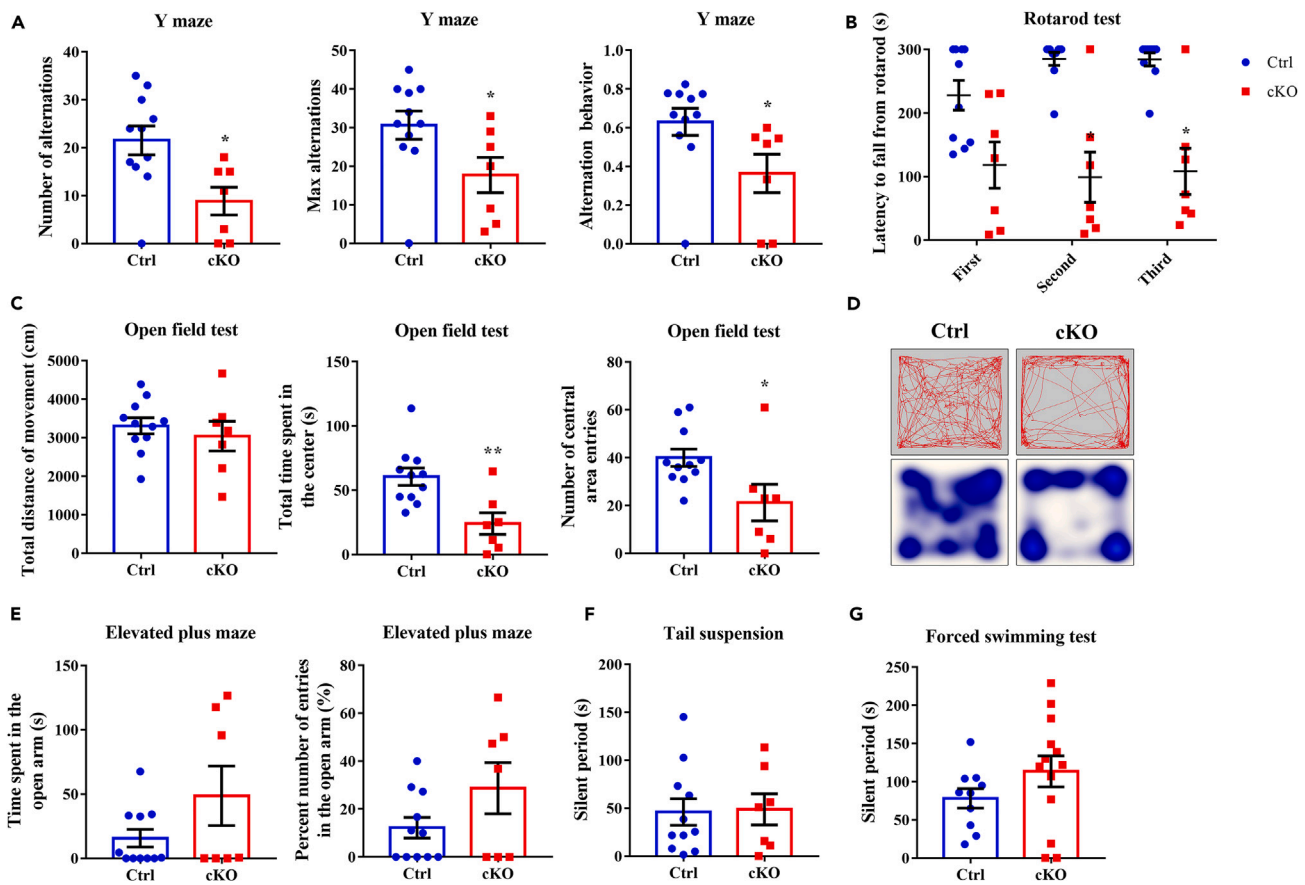


**Figure 3. SRSF10 knockout in NPCs results in impaired learning and memory ability and increased anxiety for adult mice**

Y-maze tests (A), rotarod tests (B), open-field tests (C, D), elevated plus-maze test (E), tail suspension tests (F) and forced swimming tests (G) were analyzed using the adult (2M) SRSF10 cKO and the control (Ctrl) mice. D is the representative tracks (upper panel) and heat maps (bottom panel) of open field test. Data are represented as mean  $\pm$  SEM. 7–10 two-month-old mice for each genotype were analyzed. The dots represent data from individual mice. Student's *t* test for two-tailed distribution was used for comparison of two group of samples. \**p* < 0.05, \*\**p* < 0.01.

### SRSF10 knockout or knockdown inhibits NPCs proliferation in the neocortex

Among the cortical neurons, excitatory neurons are the main components and count for approximately 80%.<sup>29</sup> During cortical neurogenesis, the excitatory neurons were generated mainly from two types of NPCs, RGCs in the VZ and IPCs in the SVZ. The RGCs undergo asymmetric cell division to self-renew as well as produce a daughter cell that is either a neuron or an IPC, while the IPCs undergo symmetric cell division to self-renew or produce neurons.<sup>5,6</sup>

Therefore, the amount and proliferation abilities of these NPCs are critical factors that affect the number of cortical neurons. To reveal whether the reduced neuron numbers in SRSF10 cKO mice cortex was caused by reduction of NPCs, we performed immunostaining for the NPC marker SOX2 and found that the number of SOX2-positive cells reduced significantly in the cortex of E14.5 cKO mice. By 2 h of EdU incorporation, we found that the ratio of EdU-positive NPCs (the ratio between the number of EdU/SOX2 double-positive cells to the number of SOX2-positive cells) also decreased significantly at E14.5 (Figures 4A and 4B), indicating that SRSF10 deletion significantly decreased the total number and proliferation ability of NPCs during the cortex development.

We further immunostained the brain sections for PAX6 and TBR2, the markers of RGCs and IPCs, respectively, and found that both the number of TBR2-positive cells and the ratio of EdU-positive cells among the IPCs (the ratio between the number of EdU/TBR2 double-positive cells to the number of TBR2-positive cells) were reduced significantly (Figure 4C) in cortex of E14.5 cKO mice, as we expected, while the number of

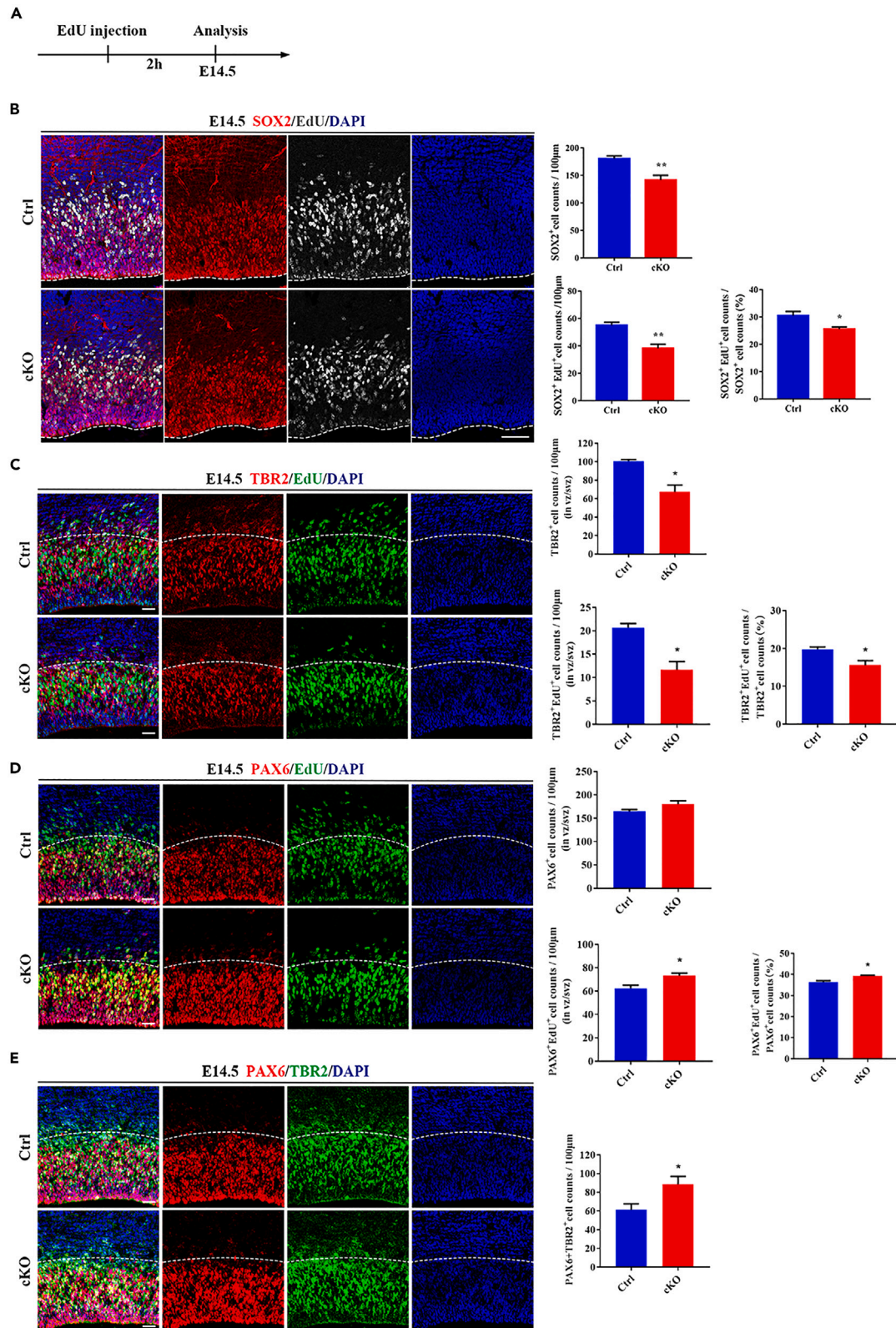


**Figure 4. SRSF10 knockout or knockdown inhibits NPCs proliferation in the neocortex**

(A) Time schedule for the EdU injection and the subsequent analysis of B to E.  
 (B–D) Double immunostaining images of EdU and the NPCs markers SOX2, TBR2, and PAX6 respectively, in the cortex of E14.5 SRSF10 cKO mice. The right panels are the corresponding statistical data.  
 (E) Representative immunostaining images (left) and the corresponding statistical data (right) of PAX6/TBR2 double-positive cells in the SRSF10 cKO and the control mouse cortex. DAPI was used to counterstain the nucleus. Scale bars represent 20  $\mu\text{m}$ . Data are represented as mean  $\pm$  SEM. At least 3 mouse brains for each genotype were analyzed. Student's t test for two-tailed distribution was used for comparison of two group of samples. \* $p < 0.05$ , \*\* $p < 0.01$ .

PAX6-positive cells at E14.5 showed no significant difference, and the ratio of EdU-positive cells among the RGCs (the ratio between the number of EdU/PAX6 double-positive cells to the number of PAX6-positive cells) was even increased slightly (Figure 4D). We also performed this analysis using *in utero* electroporation (IUE)-mediated SRSF10 knockdown in the RGCs of E14.5 mice and obtained similar results, which showed that the number of TBR2-positive cells expectedly decreased, while that of PAX6-positive cells increased among the SRSF10 knockdown (as marked by GFP positive) cells in the cortex (Figure S2).

The inconsistency alterations of the number of PAX6-positive cells with that of SOX2-positive cells remind us that an increasing partial of the PAX6-positive cells may be in the progress of transiting into TBR2-positive IPCs while still expressing PAX6. Therefore, we counted the number of PAX6/TBR2 double-positive cells, the results showed that the number of PAX6/TBR2 double-positive cells increased significantly in the SRSF10 cKO mice (Figure 4E), reminding that SRSF10 depletion may stall the cell fate transition from RGCs to IPCs.

However, when we calculated the number of PAX6-positive/TBR2-negative cells (PAX6-positive cells deducted by PAX6/TBR2 double-positive cells), we found that it showed a trend of decrease ( $-15.50 \pm 9.031$ ,  $p = 0.15$ ,  $n = 3$ ), but not increase, in the SRSF10 cKO cortex, indicating that the stall of cell fate transition may occur not at the PAX6-positive/TBR2-negative stage but at the subsequent PAX6/TBR2 double-positive stage in the cKO cortex. Combining the above-mentioned observations that both the number and the EdU incorporation ratio of SOX2-positive NPC cells decreased significantly (Figure 4B), and both the TBR2-positive (Figure 4C) and the sum of PAX-positive and TBR2-positive cells ( $-53.67 \pm 3.528$ ) decreased significantly, the decrease of PAX6-positive/TBR2-negative cells suggested that the proliferation in these cells was also inhibited.

In a word, the above results indicated that depletion of SRSF10 in NPCs decreased the total number and inhibited the proliferation ability of the NPCs in mice cortex and may stall the cell fate transition from RGCs to IPCs.

Since changes in cell numbers are associated not only with cell proliferation and cell fate transition, but may also with cell death. Therefore, we also examined the apoptosis of SRSF10-deficient NPCs. We found that although the cleaved caspase 3 (CC3) positive cells increased significantly in the neocortex of SRSF10 cKO mice at E14.5, compared with those in the corresponding control mice (Figure S3), the absolute increase in the number was much less, only  $5.556 \pm 0.9323$  in the VZ/SVZ per 100 $\mu\text{m}$  of the neocortex (Figure S3C) compared with the decrease in the number of SOX2-positive NPCs ( $38.92 \pm 9.523$  per 100 $\mu\text{m}$  of the neocortex) (Figure 4B upper right panel). Thus, the results suggested that although the increased apoptosis in the VZ/SVZ may play a part to the decrease of cortical NPCs, its contribution is very limited and not the dominant cause to induce such significant reduction in the cortical NPCs after SRSF10 cKO.

**SRSF10 knockdown inhibits the proliferation and stemness of neocortical NPCs *in vitro* and causes the abnormal cell cycle progress**

We further confirmed the involvement of SRSF10 in the proliferation of NPCs using the primary cultured mouse NPCs. We found that both the cell viability (as analyzed by CCK8) and the neurosphere-forming ability (as indicated by the number of large neurospheres formed by equal inoculation density of NPCs) decreased significantly for the SRSF10 cKO NPCs (Figure 5A). The number of BrdU-incorporated cells was reduced significantly as well (Figure 5B). These results confirmed that SRSF10 deletion reduces the proliferative capacity of NPCs *in vitro*. We also confirmed the function of SRSF10 in NPCs proliferation using recombinant lentivirus-mediated SRSF10 knockdown on adherent confluent and found that both the cell density and morphology of the NPCs was significantly altered when SRSF10 knockdown (Figure 5C). The expression levels of both PCNA, the cell proliferation marker, and SOX2, the marker for cell stemness, were decreased when SRSF10 knockdown, as revealed by Western blot (Figure 5D). All the above results indicated that SRSF10 was involved in the proliferation process of NPCs, and lack of SRSF10 reduces the proliferation ability of NPCs.

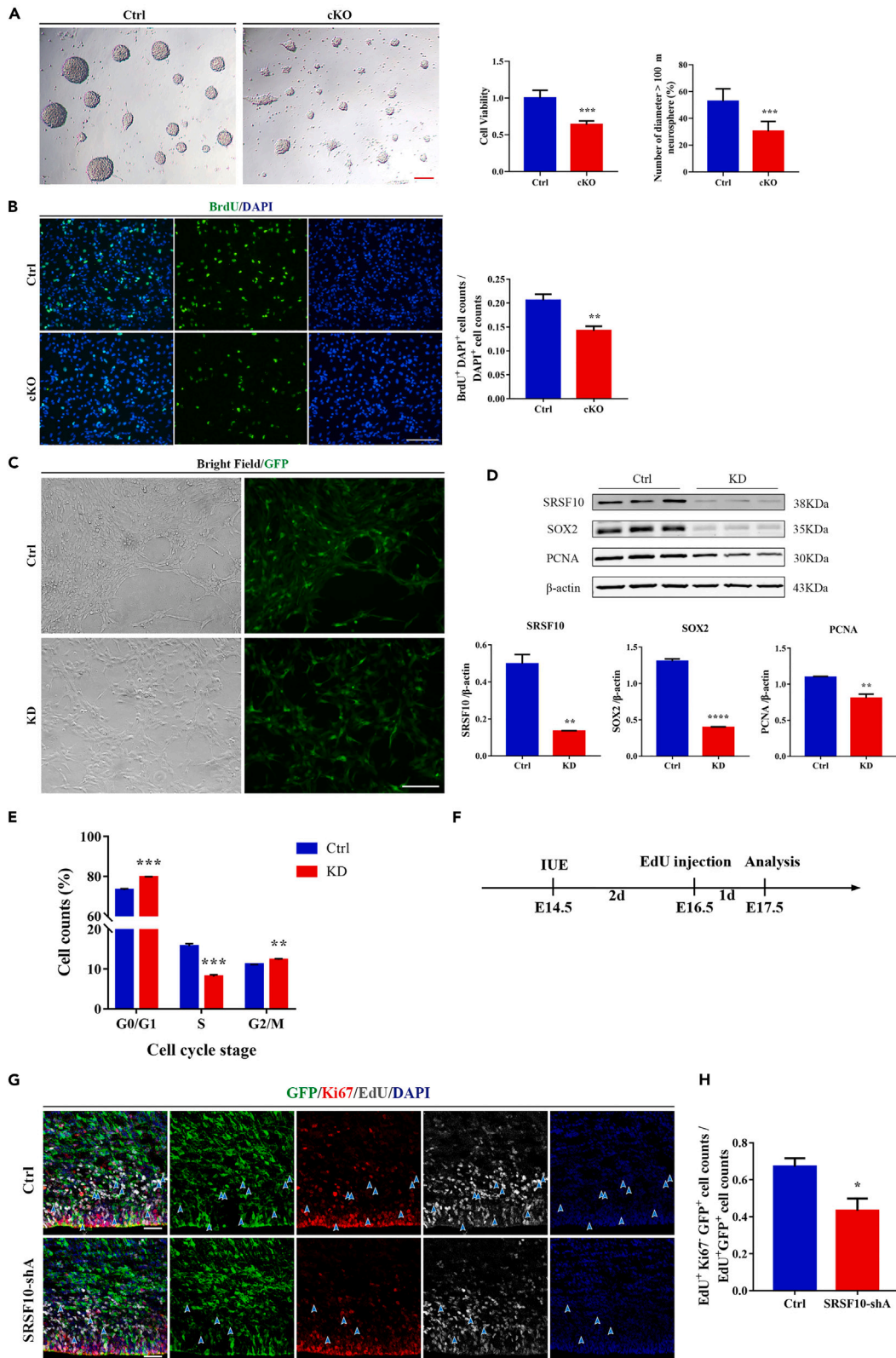


**Figure 5. SRSF10 knockdown inhibits the proliferation and the stemness of neocortical NPCs *in vitro* and causes the abnormal cell cycle progress**

(A) Bright field microscopy images of primary cultured NPCs-formed neurospheres 5 days after cell inoculation. Right panels: The statistical data of the cell viability analyzed by CCK8 and the number of neurospheres larger than 100  $\mu\text{m}$  in diameter in each well of the 96-well cell culture plate.

(B) Left panel: Immunostaining images of BrdU-incorporated NPCs showing the proliferation ability of the cells. BrdU was added into the medium of the adherent cultured primary NPCs for 1 h before the BrdU immunostaining. Right panel: Statistical data of the percent of BrdU-incorporated cells. The NPCs in A and B are derived from the E14.5 embryonic cortex of SRSF10 cKO mice (cKO) and its littermate control mice (Ctrl).

(C) Bright field and fluorescent microscopy images of NPCs indicating the cell density and morphology was significantly altered in the adherent NPCs after shRNA-mediated SRSF10 knockdown (KD).

(D) Western blots of the expression of SRSF10, SOX2, PCNA, respectively, in the SRSF10 knockdown (KD) and the control (Ctrl) cells. The expression of  $\beta$ -actin as the loading control. The columns below indicate the corresponding statistical data of the expression levels.

(E) The results of flow cytometry for cell cycle of the neocortical NPCs *in vitro*. SRSF10 knockdown (KD) induces decrease in the number of S-phase NPCs, while increase in G0/G1 and G2/M phase NPCs, compared with the control (Ctrl).

(F) Time schedule of IUE-mediated SRSF10 knockdown (SRSF10-shA) and EdU incorporation to assess cell cycle exiting for G and H.

(G) Immunostaining images of GFP, proliferation marker Ki67 and EdU to analyze cell cycle exiting of E14.5 SRSF10 KD (KD) and the control (Ctrl) mice neocortex. The NPCs which exit cell cycle (EdU positive but Ki67 negative) among the GFP positive cells were indicated by the blue arrows.

(H) The statistical data shows that the ratio of cells exiting the cell cycle (the ratio of Ki67 negative cells among the GFP/EdU double-positive cells) decreased significantly in the SRSF10 KD mouse cortex, compared with that in the Ctrl mice. DAPI was used to counterstaining the nucleus. The scale bars represent 100  $\mu\text{m}$ . Data are represented as mean  $\pm$  SEM. For analysis of cultured cells, at least 3 independent experiments were performed, and each experiment performed in triplicate. For analysis of brain sections, at least 3 mouse brains for each genotype were analyzed. Student's t test for two-tailed distribution was used for comparison of two groups of samples. \* $p < 0.05$ , \*\* $p < 0.01$ , \*\*\* $p < 0.001$ , \*\*\*\* $p < 0.0001$ .

The decrease of BrdU-labeled cell number in SRSF10 deleted NPCs reminds that SRSF10 may be involved in the cell cycle progression of NPCs. We further speculated whether lack of SRSF10 altered cell cycle progression in NPCs using lentivirus-mediated SRSF10 knockdown. Flow cytometry results showed that the number of NPCs in S phase decreased significantly when SRSF10 was knockdown, which was consistent with the results of BrdU-labeling analysis, while those of NPCs in G0/G1 phase as well as G2/M phase increased, suggesting that lack of SRSF10 caused abnormal in the cell cycle progression of NPCs (Figure 5E). In addition, using IUE, we found that the ratio of Ki67 negative cells among the EdU/GFP double-positive cell population (which stands for the NPCs exiting the cell cycle) decreased significantly in the cortex of SRSF10-knockdown mice (Figures 5F–5H), indicating that the cell cycle exit process was inhibited in the NPCs lacking SRSF10.

**SRSF10 IS REQUIRED FOR NEUROGENESIS IN DEVELOPING NEOCORTEX**

Changes in the number of NPCs can affect neurogenesis in the neocortex, so we performed immunostaining of TUJ1 (the neuronal marker) to explore whether SRSF10 deletion affects cortical neurogenesis. The results showed that the thickness of the TUJ1 positive cells-covered area tended to be thinner in the neocortex of E14.5 cKO mice, and TUJ1/GFP double-positive cells, BRN2/GFP double-positive cells were all significantly reduced in the IUE-mediated SRSF10-knockdown cortex (Figures 6A–6D), suggesting that SRSF10 deletion attenuated neocortical neurogenesis. Moreover, by tracing the EdU/GFP double-labelled cells in the cortical plate 3 days after EdU injection, we analyzed the ratio of NPCs in the terminal mitosis phase among the IUE-mediated GFP-positive NPCs. The results showed that the ratio of EdU/GFP double-positive cells among the total GFP-positive cells was significantly reduced in the cortical plate (CP) of the IUE-mediated SRSF10-knockdown mice (Figures 6E and 6F), indicating that SRSF10 knockdown reduced the number of NPCs in the terminal mitosis phase (and differentiated into neurons) significantly in E14.5 mouse cortex.

We also investigated whether SRSF10 is involved in neurogenesis *in vitro*. By analyzing the induced neuronal differentiation ability of the primary NPCs, we found that the proportion of MAP2-positive cells was significantly reduced in the NPCs isolated from SRSF10 cKO mice, compared with the control, suggesting that SRSF10 knockout reduced significantly the differentiation of NPCs into neurons (Figure S4). Overall, these data from *in vivo* and *in vitro* experiments suggest that SRSF10 is critical for maintaining of neurogenesis during neocortex development.

**SRSF10 knockdown inhibits PI3K-AKT-mTOR-CCND2 signaling pathway and alters the alternative splicing of *Nasp* in NPCs**

To further investigate the mechanisms by which SRSF10 regulates the proliferation of NPCs in cortical development, we performed global transcriptome analysis of NPCs with or without lentivirus-mediated SRSF10 knockdown. The data of RNA sequencing (RNA-seq) have been deposited into NCBI's Gene Expression Omnibus, and are accessible through GEO Series accession number GSE225647 (<https://www.ncbi.nlm.nih.gov/geo/query/acc.cgi?acc=GSE225647>). Analysis of RNA-seq data revealed that the expression level of

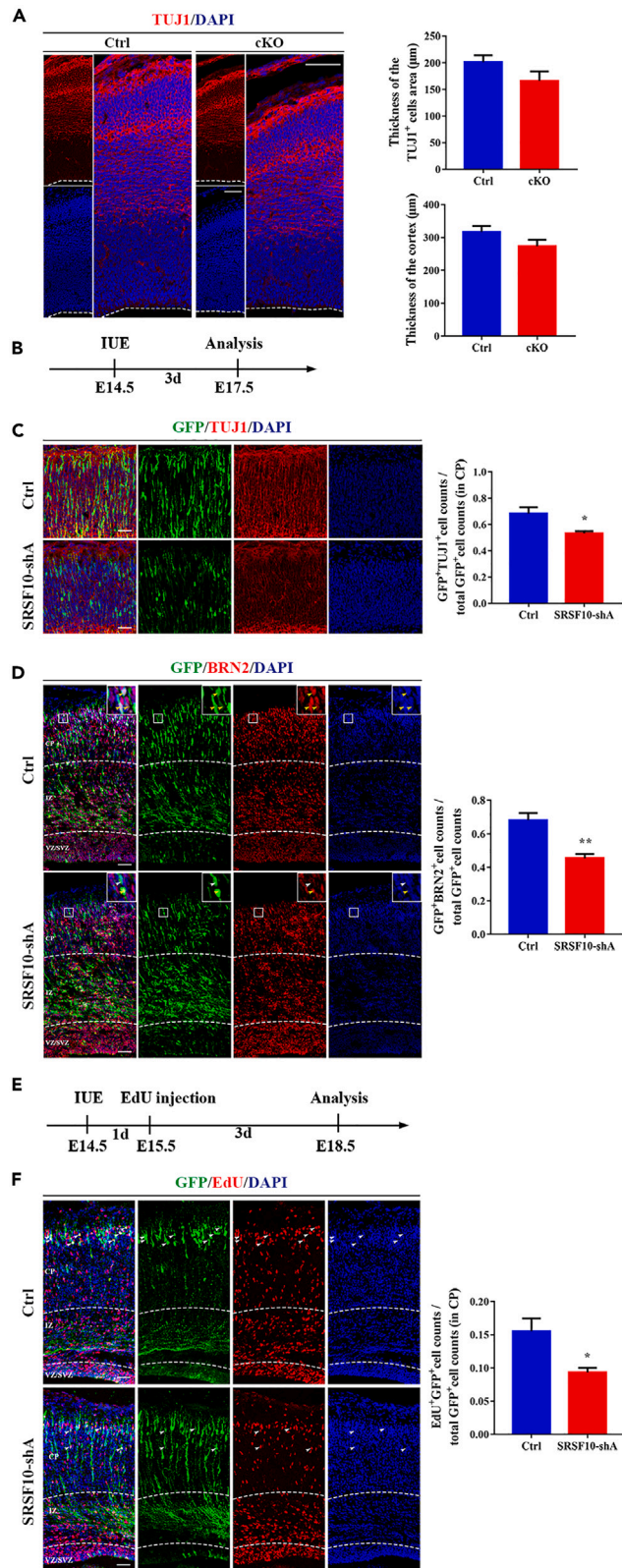


**Figure 6. SRSF10 is required for neurogenesis in developing neocortex**

(A) SRSF10 knockout in NPCs (cKO) tends to decrease the TUJ1 positive cells in the neocortex of E14.5 mice. Left panel: Immunostaining images of the neuronal marker TUJ1. Right panels: Statistical data of the thickness covered by the TUJ1 positive neurons, and the cortical thickness.

(B–D) IUE-induced SRSF10 knockdown decreases the ratio of TUJ1(C) or BRN2 (D) positive cells among the GFP-positive cells. The GFP positive indicates the cells that were transfected by SRSF10 knockdown plasmids (SRSF10-shA) or the control plasmids (Ctrl) by IUE. B shows the time schedule of IUE and the subsequent analysis for C and D. Double immunostaining of GFP and TUJ1(C) or BRN2 (D) were performed.

(E and F) IUE-induced SRSF10 knockdown (SRSF10-shA) decreased the ratio of NPCs which are in the terminal mitosis in the cortical plate (CP) of E14.5 mice. Double immunostaining of EdU and GFP 3 days after EdU injection (E) in the E14.5 mice brain was used. The right panel is the statistical ratio of EdU/GFP double-positive cells in the CP. DAPI was used for counterstaining of nucleus. The scale bars represent 50  $\mu$ m for A, C, D, and F. Data are represented as mean  $\pm$  SEM. At least 3 mouse brains for each genotype were analyzed. Student's t test for two-tailed distribution was used for comparison of two groups of samples. \*p < 0.05, \*\*p < 0.01.

multiple genes, especially cell cycle-related genes, was changed in the SRSF10-knockdown (KD) NPCs (Figure S5 & Table S1). Furthermore, the PI3K-AKT signaling pathway, which is associated with cell proliferation, was significantly down-regulated upon SRSF10 knockdown, as indicated by the Path-Act-Network analysis of the RNA-seq data (Figure S5A). Therefore, we examined the activation of PI3K-AKT-mTOR signaling pathway in the SRSF10-knockdown NPCs using Western blot analysis, the results showed that the expressions of both phosphorylated AKT and phosphorylated mTOR were significantly decreased in the SRSF10 knockdown NPCs (Figures 7A–7D), indicating that the PI3K-AKT-mTOR signaling pathway was inhibited. In addition, by RT-PCR, we found the expression of *Ccnd2*, a downstream gene of PI3K-AKT-mTOR,<sup>30</sup> was significant down-regulated in SRSF10-knockdown group (Figure 7E). These results suggest that SRSF10 may participate in the proliferation process of NPCs by regulating the PI3K-AKT-mTOR-CCND2 signaling pathway.

In addition, in RNA-seq of the P0 SRSF10 cKO mouse cortex (GEO series accession number GSE225647 as mentioned above), we found that loss of SRSF10 resulted in significant changes in the alternative splicing of *Nasp*, a critical cell proliferation-related gene,<sup>31–33</sup> by reducing the proportion of the exon7-inclusive splicing isoform (Figure 7F). In mice, there are two types of NASP proteins, tNASP and sNASP, which have been reported to possess distinct functions in cell proliferation.<sup>34,35</sup> The exon 7 is included only in the splicing variant 2 of *Nasp* mRNA that encodes tNASP protein but not in the variant 3 mRNA that encodes sNASP protein. We designed specific primers for amplifying the fragment between exon 6 and exon 8 of *Nasp* mRNA to discriminate exon7 inclusive from exon7 exclusive isoform. By RT-PCR analysis, we confirmed the significant reduction in the proportion of exon7-inclusive splicing isoform in the cortex of P0 SRSF10 cKO mice (Figures 7G and 7H). We further investigate the role of SRSF10 in *Nasp* splicing in primary NPCs using lentivirus-mediated SRSF10 knockdown. RT-PCR showed that SRSF10 knockdown decreased significantly the proportion of exon7-inclusive splicing isoform in the NPCs, as we expected (Figures 7I and 7J). Western blot analysis also showed that SRSF10 knockdown in NPCs decreased the expression level of tNASP protein (which contains the exon7-encoded amino acid sequence), and the ratio of tNASP protein to sNASP protein as well (Figures 7K and 7L).

To investigate whether the SRSF10 functions directly on *Nasp* splicing, we performed RNA immunoprecipitation using SRSF10 antibody. We found that the *Nasp* mRNA has a significantly enrichment in the immunoprecipitation complex (Figures 7M and 7N, SRSF10), compared with the negative control (IgG), indicating that *Nasp* mRNA was bound directly by SRSF10 in NPCs.

The above findings suggest that during cortex development, SRSF10 probably regulates tNASP expression and further regulates the proliferation of NPCs via regulating the alternative splicing of *Nasp* exon 7.

## DISCUSSION

In this study, we investigated the function and mechanism of SRSF10 in the proliferation and neurogenesis of NPCs during mouse neocortex development. By conditional depleting SRSF10 in NPCs *in vivo* and *in vitro*, we found that dysfunction of SRSF10 leads to developmental defects of the brain, with abnormal ventricle enlargement and cortical thinning anatomically, and decreased NPCs proliferation and weakened cortical neurogenesis histologically. We also detected the altered behavior in the SRSF10 cKO mice, with impaired learning and memory ability and increased anxiety. Furthermore, we proved that the function of

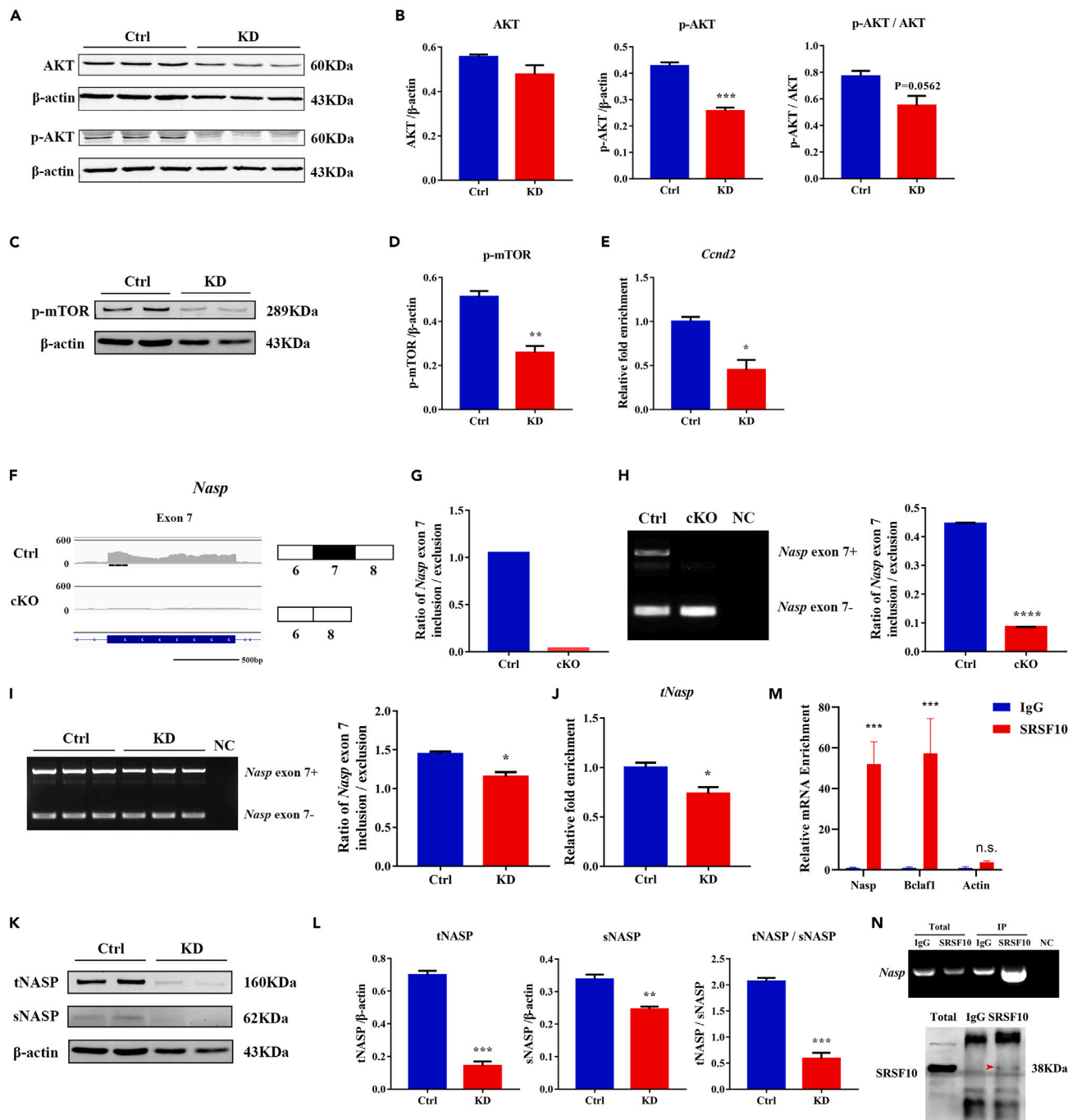


**Figure 7. SRSF10 knockdown inhibits PI3K-AKT-mTOR signaling pathway and alters the alternative splicing of *Nasp* in NPCs**

(A–E) The PI3K-AKT-mTOR signaling pathway was inhibited in SRSF10 knockdown primary NPCs (KD), compared with the control NPCs (Ctrl). The expressions of AKT, p-AKT (A, B) and p-mTOR (C, D) were analyzed by Western blot analysis. The expression of *Cnd2* (E) were analyzed by RT-qPCR. B and D are statistical data for A and C, respectively. p-AKT and p-mTOR, phosphorylated AKT and TOR, respectively.

(F–H) The ratio of exon7-inclusive splicing isoform of *Nasp* gene was significantly decreased in the cortex of P0 SRSF10 cKO mice (cKO), compared with the littermate control mice (Ctrl), analyzed by RNA-Seq (F, G) and RT-PCR (H). G shows the ratio of *Nasp* exon7-inclusive to exon7-exclusive isoforms of F. The right panel in H is the statistical data of the RT-PCR (left panel).

(I–L) The ratio of both exon7-inclusive splicing isoform and tNASP protein (which contains exon7-encoded peptide sequence) were decreased significantly in the lentivirus-mediated SRSF10-knockdown NPCs (KD), analyzed by RT-PCR (I, J) and Western blot (K, L). The right panel in I is the statistical data of the RT-PCR (left panel). J is the statistical results of RT-qPCR of tNasp isoform. L is the statistical data of Western blot (K) showing the expression of tNASP and sNASP protein isoforms, and the ratio of tNASP/sNASP, respectively. H<sub>2</sub>O was used as a negative control sample (NC). (M, N). RNA immunoprecipitation

**Figure 7. Continued**

(RIP) results showing that *Nasp* mRNA has enrichment in the immunoprecipitation (IP) complex of SRSF10 antibody (IgG as the negative control). The statistical data of RT-qPCR for *Nasp* (M), the representative RT-PCR image of *Nasp* (N, upper panel) and Western blot analysis confirming the existence of SRSF10 protein in the SRSF10 IP complex (N, bottom panel). Data are represented as mean  $\pm$  SEM. At least 3 independent experiments were performed for each genotype, and each experiment performed in triplicate. Student's *t* test for two-tailed distribution was used for comparison of two groups of samples. \**p* < 0.05, \*\**p* < 0.01, \*\*\**p* < 0.001, \*\*\*\**p* < 0.0001.

SRSF10 on NPCs proliferation involved the regulation of PI3K-AKT-mTOR-CCND2 pathway and the alternative splicing of *Nasp*, a gene encoding isoforms of cell cycle regulators.

Among the developmental defectives in the NPCs-specific SRSF10-knockout mice, similar characteristics, including the enlarged ventricle and thinned neocortex, are also displayed in several human brain developmental diseases such as congenital hydrocephalus and microcephaly.<sup>36–38</sup> Besides, the decreased expression of *Ccnd2*, a downstream gene of PI3K-AKT-mTOR pathway which encodes a critical cell cycle-regulating protein,<sup>30,39</sup> may also be associated with the microcephaly pathogenesis, because *Ccnd2* loss of function owing to a variation has been reported to be a cause of microcephaly.<sup>37</sup> Therefore, our results suggest that SRSF10 deficiency may be involved in the pathogenesis of these diseases, and maintaining the normative expression of SRSF10 in NPCs is essential for cerebral development. Previous work has reported that SRSF10 is involved in the development of several other types of tissues such as striated muscle development, myoblast differentiation, and adipocyte differentiation,<sup>40,41</sup> the results of present work extended the potential function of SRSF10 in neural development and neural defective diseases.

In this study, besides multiple *in vivo* and *in vitro* data supporting the SRSF10 KO-induced inhibition of NPCs proliferation, a seemingly inconsistent data of increase in the number of PAX6-positive cells also presented in the E14.5 SRSF10 cKO cortex (Figures 4D and S2D), which implied that the cell fate transition from RGCs to IPCs may be stalled. Meanwhile, the calculating data of the SRSF10 KO-induced change of PAX6-positive/TBR2-negative cells (from the data of Figures 4C–4E) showed a decrease trend, indicating that the stall may occur at the PAX6/TBR2 double-positive stage but not at the PAX6-positive/TBR2-negative stage. How and to what extent the KO-induced stalling of cell fate transition functions in the cortical development needs further investigation.

In view of the significant reduction of cortical thickness in the SRSF10 cKO mice, we examined the number of different types of excitatory neurons in the neocortex to better explore the alterations in the SRSF10 cKO mice. It is well known that excitatory neurons in mouse cerebral cortex have six distinct anatomical layers, which are generated in an “inside out” pattern during the developmental process.<sup>42</sup> The immunostaining of SRSF10 cKO mice cortex at multiple developmental stages showed that SRSF10 deletion resulted in decreases not only in TBR1 and CTIP2 positive deep-layer neurons, but also in BRN2 positive superficial neurons. As NPCs neurogenesis and neuronal migration are the two major processions that affect neuronal development,<sup>43,44</sup> the significantly reduced numbers of various layers of excitatory neurons implied that the major cause of the thinning cortical in the SRSF10 cKO mice may be the insufficient neurogenesis rather than disordered neuronal migration.

Besides the NPCs in the VZ/SVZ regions which produce excitatory neurons, the NPCs in the MGE, which produce the GABAergic neurons of the cortex, also contribute to the generation of cortical neurons.<sup>45</sup> In order to reveal whether the SRSF10 deletion in MGE NPCs also contributes to the reduction in the number of cortical neurons in adult mice, we analyzed the GABAergic neurons using the immunostaining of GABA in 2-month-old mouse cortex and found that the number of GABAergic neurons decreases significantly in the SRSF10 cKO cortex, compared with the non-KO control (data not shown), indicating the contribution of SRSF10 deletion in the MGE NPCs to the reduced numbers of neurons in adult cortex. However, by comparing the decrease amplitude between the total neurons and GABAergic neurons in adult cortex, we found that the decrease in the number of GABAergic neurons is much less than that of the total neurons (Figure 2C upper panel) indicated by NeuN immunostaining. Thus, the SRSF10 deletion in the VZ/SVZ NPCs that produce excitatory neurons may still contribute to the majority of the reduced numbers of neurons in the cortex of adult cKO mice. This conclusion is also supported by the significant decrease in the numbers of excitatory neurons of different cortical layers in the adult mice (Figures 2F, 2G, 2J, and 2K), which does not contain the GABAergic neurons. Besides, the IUE analysis (Figures 6C and 6D) also showed that plasmid-mediated knockdown of SRSF10 in a portion of the VZ NPCs causes the significant decrease in the numbers of excitatory neurons of different cortical layers, which also supports this conclusion.

As a neural-tissue highly expressed protein, SRSF10 express ubiquitously in neurons, astrocytes as well as in NPCs. Therefore, in the neocortex of Nestin-Cre SRSF10 cKO mice, in addition to the decrease in the expression of SRSF10 in NPCs, the decrease also presented in neurons and astrocytes as well, which were derived from the NPCs. The effect of SRSF10 decrease in neurons and astrocytes may also contribute to the impaired neurogenesis and enlarged ventricle in the adult SRSF10 cKO mouse neocortex. To further confirm the contribution of SRSF10 in NPCs, we retraced the neurogenesis to as early as in E14.5 mouse cortex (Figures 2, and 6) in the SRSF10 cKO mice, when the neurogenesis was at the early stage and the gliogenesis has not been started, in an attempt to reduce the effect of SRSF10 reduction in neurons and astrocytes. We observed significant reduced neuronal numbers for each layer in the cortex of E14.5 cKO mice (Figure 2), indicating that the deficiency of SRSF10 protein in NPCs exerts dominant effects on the impaired neurogenesis of neocortex.

In this study, we found that lacking of SRSF10 decreases the expression of exon7-inclusive *tNasp* and the ratio of exon7 inclusive to exclusive *Nasp* (*tNasp/sNasp*) in the NPCs-specific SRSF10 cKO mouse cortex as well as in the primary NPCs. The results suggest that as a pre-mRNA splicing factor, SRSF10 may function in the NPCs via promoting the exon7 inclusive alternative splicing of *Nasp* and increase the expression of *tNasp* isoform. The tNASP, the longer protein isoform of NASP which contains the exon7 encoded sequence, is reported to be required for the normal cell cycle progression via binding to the histone protein and facilitate the chromosome reassembly after DNA replication,<sup>31,46</sup> while the s-NASP, the shorter isoform of NASP which differs from the t-NASP in lacking a histone protein-binding site and two ATP/GTP-binding sites, the important sites for the functional attribution of tNASP in chromatin reassembly, has no such function. Combining the decreased *tNasp* isoform expression with the altered cell cycle progression and the inhibited proliferation in the NPCs after SRSF10 knockdown or knockout, our results suggest that the SRSF10 probably functions in the proliferation of NPCs during mouse cortical development via promoting the exon7-inclusive splicing of *Nasp* and regulating the cell cycle progression. The exact mechanisms need further investigation.

In investigating the mechanism under the SRSF10 knockout or knockdown-induced decrease of cortical development, we observed down-regulated PI3K-AKT-mTOR pathway as well as the altered alternative splicing of *Nasp* upon SRSF10 knockout or knockdown, both of which directed to the regulation of cell proliferation and cell cycle, and both were consistent with our *in vivo* and *in vitro* observations that SRSF10 knockout or knockdown significantly decreased the proliferation and inhibited the cell cycle of NPCs. These results suggested that the regulations of both the PI3K-AKT-mTOR-CCND2 pathway and the alternative splicing of *Nasp* are involved in the function of SRSF10 in regulating of proliferation and cell cycle of NPCs, although further investigations are needed to reveal whether or how the PI3K-AKT-mTOR signal pathway links mechanistically to the alternative splicing of *Nasp*.

Studies indicate that the impact of SRSF10 on alternative splicing depends on the position of the putative SRSF10-binding motifs on the target pre-mRNAs.<sup>47</sup> When SRSF10 binds to the motif in the cassette exon, it tends to promote inclusion of this exon. AAAGACAAA is a consensus SRSF10-binding sequence that can be recognized and bound with high affinity by SRSF10 which benefits the inclusive splicing of this exon.<sup>26,48</sup> We analyzed the nucleotide sequence of mouse *Nasp* exon7 and found a sequence of GAAGACAAA highly resembles this consensus motif. Thus, we deduce that SRSF10 may promote the exon7-inclusive splicing of *Nasp* by recognizing and binding to this motif. Our RNA immunoprecipitation results indicating the binding of SRSF10 protein with the *Nasp* pre-mRNA in the NPCs also support this deduction.

In conclusion, the present study extended our knowledge in the function of the splicing factor SRSF10 in NPCs and in the development of neocortex. The study highlights the necessity of SRSF10 expression in the formation of a structurally and functionally normal neocortex. To our knowledge, this is the first time to report the function of SRSF10 in proliferation of NPCs as well as development of neocortex.

### Limitations of the study

There are several limitations in this study. Although we found that SRSF10 is involved in the regulation of PI3K-AKT-mTOR signaling pathway, how SRSF10 is directly linked to the regulation of this pathway keeps unclear. Further investigations are needed to reveal the target gene whose pre-mRNA splicing is regulated by SRSF10 and therefore affect the activation of this signal pathway. Besides, owing to the lack of related reports so far, whether the SRSF10 deletion-induced alteration of *Nasp* pre-mRNA alternative splicing is involved in the regulation of PI3K-AKT-mTOR signaling pathway is still unknown and needs to be revealed. In addition, owing to the observation that the stalling of cell fate transition from PAX6 positive RGCs to

TRB2 positive IPCs may also occur in the SRSF10 cKO mouse cortex in addition to the proliferation inhibition of these NPCs, further investigations are also needed to reveal to what extent does the installation function in the cortex development.

## STAR★METHODS

Detailed methods are provided in the online version of this paper and include the following:

- KEY RESOURCES TABLE
- RESOURCE AVAILABILITY
  - Lead contact
  - Materials availability
  - Data and code availability
- EXPERIMENTAL MODEL AND STUDY PARTICIPANT DETAILS
  - Experimental animals
  - Generation of SRSF10 conditional knockout mice
  - Construction of recombinant pSuper plasmid and lentivirus for SRSF10 knockdown
- METHOD DETAILS
  - In utero electroporation
  - EdU/BrdU labeling
  - Cell culture
  - Cell transfection and infection
  - Immunofluorescent labeling of brain sections and cells
  - Western blotting
  - RT-PCR
  - RNA-immunoprecipitation (RIP)
  - Cell cycle analysis
  - RNA sequencing and bioinformatic analysis
  - Behavioral testing
  - Confocal imaging
- QUANTIFICATION AND STATISTICAL ANALYSIS
  - Data and software availability

## SUPPLEMENTAL INFORMATION

Supplemental information can be found online at <https://doi.org/10.1016/j.isci.2023.107042>.

## ACKNOWLEDGMENTS

We thank Dr. Y. Xie for providing constructive suggestions for this work. We thank Dr. J. Wang for critically reading the manuscript. This work was supported by the National Natural Science Foundation of China (grant numbers 31771112, 31571037, 81901259), Natural Science Foundation of Shanghai (23ZR1412700), Shanghai Municipal Science and Technology Major Project (No. 2018SHZDZX01), ZJ Lab, Shanghai Center for Brain Science and Brain-Inspired Technology, and Top Talent Support Program for young and middle-aged people of Wuxi Health Committee (HB2020015).

## AUTHOR CONTRIBUTIONS

X.C., J.L., and Y.M. conceived and designed the project. J.L., H.J., and Y.M. performed the experiments with helps from Z.W., A.M., and M.S. X.C., J.L., Y.M., and H.J. analyzed the data and wrote the manuscript. C.Z. and J.Z. analyzed the data and gave comments on the manuscript.

## DECLARATION OF INTERESTS

The authors declare no competing interests.

Received: January 9, 2023

Revised: April 25, 2023

Accepted: June 1, 2023

Published: June 7, 2023

REFERENCES

- Bystron, I., Blakemore, C., and Rakic, P. (2008). Development of the human cerebral cortex: boulder Committee revisited. *Nat. Rev. Neurosci.* 9, 110–122. <https://doi.org/10.1038/nrn2252>.
- Kalebic, N., and Huttner, W.B. (2020). Basal progenitor morphology and neocortex evolution. *Trends Neurosci.* 43, 843–853. <https://doi.org/10.1016/j.tins.2020.07.009>.
- Fernández, V., Llinares-Benadero, C., and Borrell, V. (2016). Cerebral cortex expansion and folding: what have we learned? *EMBO J.* 35, 1021–1044. <https://doi.org/10.15252/embj.201593701>.
- Chou, F.S., Li, R., and Wang, P.S. (2018). Molecular components and polarity of radial glial cells during cerebral cortex development. *Cell. Mol. Life Sci.* 75, 1027–1041. <https://doi.org/10.1007/s00018-017-2680-0>.
- Taverna, E., Götz, M., and Huttner, W.B. (2014). The cell biology of neurogenesis: toward an understanding of the development and evolution of the neocortex. *Annu. Rev. Cell Dev. Biol.* 30, 465–502. <https://doi.org/10.1146/annurev-cellbio-101011-155801>.
- Holguera, I., and Desplan, C. (2018). Neuronal specification in space and time. *Science* 362, 176–180. <https://doi.org/10.1126/science.aas9435>.
- Lim, L., Mi, D., Llorca, A., and Marín, O. (2018). Development and functional diversification of cortical interneurons. *Neuron* 100, 294–313. <https://doi.org/10.1016/j.neuron.2018.10.009>.
- Zhang, X., Chen, M.H., Wu, X., Kodani, A., Fan, J., Doan, R., Ozawa, M., Ma, J., Yoshida, N., Reiter, J.F., et al. (2016). Cell-Type-specific alternative splicing governs cell fate in the developing cerebral cortex. *Cell* 166, 1147–1162.e15. <https://doi.org/10.1016/j.cell.2016.07.025>.
- Aygün, N., Elwell, A.L., Liang, D., Lafferty, M.J., Cheek, K.E., Courtney, K.P., Mory, J., Hadden-Ford, E., Krupa, O., de la Torre-Ubieta, L., et al. (2021). Brain-trait-associated variants impact cell-type-specific gene regulation during neurogenesis. *Am. J. Hum. Genet.* 108, 1647–1668. <https://doi.org/10.1016/j.ajhg.2021.07.011>.
- Hwang, I., Cao, D., Na, Y., Kim, D.Y., Zhang, T., Yao, J., Oh, H., Hu, J., Zheng, H., Yao, Y., and Paik, J. (2018). Far upstream element-binding protein 1 regulates LSD1 alternative splicing to promote terminal differentiation of neural progenitors. *Stem Cell Rep.* 10, 1208–1221. <https://doi.org/10.1016/j.stemcr.2018.02.013>.
- Liu, Y., Luo, Y., Shen, L., Guo, R., Zhan, Z., Yuan, N., Sha, R., Qian, W., Wang, Z., Xie, Z., et al. (2020). Splicing factor SRSF1 is essential for satellite cell proliferation and postnatal maturation of neuromuscular junctions in mice. *Stem Cell Rep.* 15, 941–954. <https://doi.org/10.1016/j.stemcr.2020.08.004>.
- Calarco, J.A., Superina, S., O'Hanlon, D., Gabut, M., Raj, B., Pan, Q., Skalska, U., Clarke, L., Gelinas, D., van der Kooy, D., et al. (2009). Regulation of vertebrate nervous system alternative splicing and development by an SR-related protein. *Cell* 138, 898–910. <https://doi.org/10.1016/j.cell.2009.06.012>.
- Ortiz-Sánchez, P., Villalba-Orero, M., López-Olañeta, M.M., Larrasa-Alonso, J., Sánchez-Cabo, F., Martí-Gómez, C., Camafeita, E., Gómez-Salineró, J.M., Ramos-Hernández, L., Nielsen, P.J., et al. (2019). Loss of SRSF3 in cardiomyocytes leads to decapping of contraction-related mRNAs and severe systolic dysfunction. *Circ. Res.* 125, 170–183. <https://doi.org/10.1161/CIRCRESAHA.118.314515>.
- Liu, L., Chen, X.H., Huang, J., Lin, J.J., Lin, W.M., and Xu, P. (2004). NNSR1 promotes neuronal differentiation of mouse embryonic carcinoma P19 cells. *Neuroreport* 15, 823–828. <https://doi.org/10.1097/00001756-200404090-00017>.
- Liu, K.J., and Harland, R.M. (2005). Inhibition of neurogenesis by SRp38, a neuroD-regulated RNA-binding protein. *Development* 132, 1511–1523. <https://doi.org/10.1242/dev.01703>.
- Qi, Y., Li, Y., Cui, S.C., Zhao, J.J., Liu, X.Y., Ji, C.X., Sun, F.Y., Xu, P., and Chen, X.H. (2015). Splicing factor NNSR1 reduces neuronal injury after mouse transient global cerebral ischemia. *Glia* 63, 826–845. <https://doi.org/10.1002/glia.22787>.
- Xiao, P.J., Hu, L., Li, J., Lin, W., Chen, X., and Xu, P. (2007). NNSR1 is regulated in testes development and cryptorchidism and promotes the exon 5-included splicing of CREB transcripts. *Mol. Reprod. Dev.* 74, 1363–1372. <https://doi.org/10.1002/mrd.20719>.
- Frederiksen, S.B., Holm, L.L., Larsen, M.R., Doktor, T.K., Andersen, H.S., Hastings, M.L., Hua, Y., Krainer, A.R., and Andresen, B.S. (2021). Identification of SRSF10 as a regulator of SMN2 ISS-N1. *Hum. Mutat.* 42, 246–260. <https://doi.org/10.1002/humu.24149>.
- Komatsu, M., Kominami, E., Arahata, K., and Tsukahara, T. (1999). Cloning and characterization of two neural-salient serine/arginine-rich (NNSR) proteins involved in the regulation of alternative splicing in neurones. *Gene Cell.* 4, 593–606. <https://doi.org/10.1046/j.1365-2443.1999.00286.x>.
- Liu, X., Shen, S., Zhu, L., Su, R., Zheng, J., Ruan, X., Shao, L., Wang, D., Yang, C., and Liu, Y. (2020). SRSF10 inhibits biogenesis of circ-ATXN1 to regulate glioma angiogenesis via miR-526b-3p/MMP2 pathway. *J. Exp. Clin. Cancer Res.* 39, 121. <https://doi.org/10.1186/s13046-020-01625-8>.
- Chang, C., Rajasekaran, M., Qiao, Y., Dong, H., Wang, Y., Xia, H., Deivasigamani, A., Wu, M., Sekar, K., Gao, H., et al. (2022). The aberrant upregulation of exon 10-inclusive SREK1 through SRSF10 acts as an oncogenic driver in human hepatocellular carcinoma. *Nat. Commun.* 13, 1363. <https://doi.org/10.1038/s41467-022-29016-x>.
- Liu, F., Dai, M., Xu, Q., Zhu, X., Zhou, Y., Jiang, S., Wang, Y., Ai, Z., Ma, L., Zhang, Y., et al. (2018). SRSF10-mediated IL1RAP alternative splicing regulates cervical cancer oncogenesis via miL1RAP-NF-kappaB-CD47 axis. *Oncogene* 37, 2394–2409. <https://doi.org/10.1038/s41388-017-0119-6>.
- Alcantara Llaguno, S., Chen, J., Kwon, C.H., Jackson, E.L., Li, Y., Burns, D.K., Alvarez-Buylla, A., and Parada, L.F. (2009). Malignant astrocytomas originate from neural stem/progenitor cells in a somatic tumor suppressor mouse model. *Cancer Cell* 15, 45–56. <https://doi.org/10.1016/j.ccr.2008.12.006>.
- Korber, V., Yang, J., Barah, P., Wu, Y., Stichel, D., Gu, Z., Fletcher, M.N.C., Jones, D., Hentschel, B., Lamszus, K., et al. (2019). Evolutionary trajectories of IDH(WT) glioblastomas reveal a common Path of early tumorigenesis instigated years ahead of initial diagnosis. *Cancer Cell* 35, 692–704.e612. <https://doi.org/10.1016/j.ccell.2019.02.007>.
- Fushimi, K., Osumi, N., and Tsukahara, T. (2005). NNSRs/TASRs/SRp38s function as splicing modulators via binding to pre-mRNAs. *Gene Cell.* 10, 531–541. <https://doi.org/10.1111/j.1365-2443.2005.00855.x>.
- Shin, C., and Manley, J.L. (2002). The SR protein SRp38 represses splicing in M phase cells. *Cell* 111, 407–417. [https://doi.org/10.1016/s0092-8674\(02\)01038-3](https://doi.org/10.1016/s0092-8674(02)01038-3).
- Liu, X., Zheng, Y., Xiao, M., Chen, X., Zhu, Y., Xu, C., Wang, F., Liu, Z., and Cao, K. (2022). SRSF10 stabilizes CDC25A by triggering exon 6 skipping to promote hepatocarcinogenesis. *J. Exp. Clin. Cancer Res.* 41, 353. <https://doi.org/10.1186/s13046-022-02558-0>.
- Kriegstein, A., and Alvarez-Buylla, A. (2009). The glial nature of embryonic and adult neural stem cells. *Annu. Rev. Neurosci.* 32, 149–184. <https://doi.org/10.1146/annurev.neuro.051508.135600>.
- Han, W., and Sestan, N. (2013). Cortical projection neurons: sprung from the same root. *Neuron* 80, 1103–1105. <https://doi.org/10.1016/j.neuron.2013.11.016>.
- Balcazar, N., Sathyamurthy, A., Elghazi, L., Gould, A., Weiss, A., Shiojima, I., Walsh, K., and Bernal-Mizrachi, E. (2009). mTORC1 activation regulates beta-cell mass and proliferation by modulation of cyclin D2 synthesis and stability. *J. Biol. Chem.* 284, 7832–7842. <https://doi.org/10.1074/jbc.M807458200>.
- Richardson, R.T., Alekseev, O.M., Grossman, G., Widgren, E.E., Thresher, R., Wagner, E.J., Sullivan, K.D., Marzluff, W.F., and O'Rand, M.G. (2006). Nuclear autoantigenic sperm protein (NASP), a linker histone chaperone that is required for cell proliferation. *J. Biol. Chem.* 281, 21526–21534. <https://doi.org/10.1074/jbc.M603816200>.

32. Fang, J., Wang, H., Xi, W., Cheng, G., Wang, S., Su, S., Zhang, S., Deng, Y., Song, Z., Xu, A., et al. (2015). Downregulation of tNASP inhibits proliferation through regulating cell cycle-related proteins and inactive ERK/MAPK signal pathway in renal cell carcinoma cells. *Tumour Biol.* 36, 5209–5214. <https://doi.org/10.1007/s13277-015-3177-9>.
33. Yu, B., Chen, X., Li, J., Gu, Q., Zhu, Z., Li, C., Su, L., and Liu, B. (2017). microRNA-29c inhibits cell proliferation by targeting NASP in human gastric cancer. *BMC Cancer* 17, 109. <https://doi.org/10.1186/s12885-017-3096-9>.
34. Richardson, R.T., Bencic, D.C., and O’Rand, M.G. (2001). Comparison of mouse and human NASP genes and expression in human transformed and tumor cell lines. *Gene* 274, 67–75. [https://doi.org/10.1016/s0378-1119\(01\)00605-9](https://doi.org/10.1016/s0378-1119(01)00605-9).
35. Finn, R.M., Ellard, K., Eirín-López, J.M., and Ausió, J. (2012). Vertebrate nucleoplasmin and NASP: egg histone storage proteins with multiple chaperone activities. *Faseb. J.* 26, 4788–4804. <https://doi.org/10.1096/fj.12-216663>.
36. Jin, S.C., Dong, W., Kundishora, A.J., Panchagnula, S., Moreno-De-Luca, A., Furey, C.G., Allocco, A.A., Walker, R.L., Nelson-Williams, C., Smith, H., et al. (2020). Exome sequencing implicates genetic disruption of prenatal neuro-gliogenesis in sporadic congenital hydrocephalus. *Nat. Med.* 26, 1754–1765. <https://doi.org/10.1038/s41591-020-1090-2>.
37. Pirozzi, F., Lee, B., Horsley, N., Burkardt, D.D., Dobyns, W.B., Graham, J.M., Jr., Dentici, M.L., Cesario, C., Schallner, J., Pormann, J., et al. (2021). Proximal variants in CCND2 associated with microcephaly, short stature, and developmental delay: a case series and review of inverse brain growth phenotypes. *Am. J. Med. Genet.* 185, 2719–2738. <https://doi.org/10.1002/ajmg.a.62362>.
38. Ding, W., Wu, Q., Sun, L., Pan, N.C., and Wang, X. (2019). Cenpj regulates cilia disassembly and neurogenesis in the developing mouse cortex. *J. Neurosci.* 39, 1994–2010. <https://doi.org/10.1523/JNEUROSCI.1849-18.2018>.
39. Juric-Sekhar, G., and Hevner, R.F. (2019). Malformations of cerebral cortex development: molecules and mechanisms. *Annu. Rev. Pathol.* 14, 293–318. <https://doi.org/10.1146/annurev-pathmechdis-012418-012927>.
40. Wei, N., Cheng, Y., Wang, Z., Liu, Y., Luo, C., Liu, L., Chen, L., Xie, Z., Lu, Y., and Feng, Y. (2015). SRSF10 plays a role in myoblast differentiation and glucose production via regulation of alternative splicing. *Cell Rep.* 13, 1647–1657. <https://doi.org/10.1016/j.celrep.2015.10.038>.
41. Li, H., Cheng, Y., Wu, W., Liu, Y., Wei, N., Feng, X., Xie, Z., and Feng, Y. (2014). SRSF10 regulates alternative splicing and is required for adipocyte differentiation. *Mol. Cell Biol.* 34, 2198–2207. <https://doi.org/10.1128/MCB.01674-13>.
42. Cadwell, C.R., Bhaduri, A., Mostajo-Radji, M.A., Keefe, M.G., and Nowakowski, T.J. (2019). Development and arealization of the cerebral cortex. *Neuron* 103, 980–1004. <https://doi.org/10.1016/j.neuron.2019.07.009>.
43. Silva, C.G., Peyre, E., and Nguyen, L. (2019). Cell migration promotes dynamic cellular interactions to control cerebral cortex morphogenesis. *Nat. Rev. Neurosci.* 20, 318–329. <https://doi.org/10.1038/s41583-019-0148-y>.
44. Klingler, E., Francis, F., Jabaudon, D., and Cappello, S. (2021). Mapping the molecular and cellular complexity of cortical malformations. *Science* 371, eaba4517. <https://doi.org/10.1126/science.aba4517>.
45. Markram, H., Toledo-Rodriguez, M., Wang, Y., Gupta, A., Silberberg, G., and Wu, C. (2004). Interneurons of the neocortical inhibitory system. *Nat. Rev. Neurosci.* 5, 793–807. <https://doi.org/10.1038/nrn1519>.
46. Alekseev, O.M., Richardson, R.T., and O’Rand, M.G. (2009). Linker histones stimulate HSPA2 ATPase activity through NASP binding and inhibit CDC2/Cyclin B1 complex formation during meiosis in the mouse. *Biol. Reprod.* 81, 739–748. <https://doi.org/10.1095/biolreprod.109.076497>.
47. Zhou, X., Wu, W., Li, H., Cheng, Y., Wei, N., Zong, J., Feng, X., Xie, Z., Chen, D., Manley, J.L., et al. (2014). Transcriptome analysis of alternative splicing events regulated by SRSF10 reveals position-dependent splicing modulation. *Nucleic Acids Res.* 42, 4019–4030. <https://doi.org/10.1093/nar/gkt1387>.
48. Wu, W., Zong, J., Wei, N., Cheng, J., Zhou, X., Cheng, Y., Chen, D., Guo, Q., Zhang, B., and Feng, Y. (2018). CASH: a constructing comprehensive splice site method for detecting alternative splicing events. *Briefings Bioinf.* 19, 905–917. <https://doi.org/10.1093/bib/bbx034>.
49. Vomund, S., Sapir, T., Reiner, O., de Souza Silva, M.A., and Korth, C. (2013). Generation of topically transgenic rats by in utero electroporation and in vivo bioluminescence screening. *J. Vis. Exp.* e50146. <https://doi.org/10.3791/50146>.
50. Louis, S.A., and Reynolds, B.A. (2010). Neurosphere and neural colony-forming cell assays. In *Protocols for Neural Cell Culture*, Fourth Edition, L.C. Doering, ed., pp. 1–28. [https://doi.org/10.1007/978-1-60761-292-6\\_1](https://doi.org/10.1007/978-1-60761-292-6_1).
51. Ratnadiwakara, M., and Änkö, M.L. (2018). RNA immunoprecipitation assay to determine the specificity of SRSF3 binding to nanog mRNA. *Bio. Protoc.* 8, e3071. <https://doi.org/10.21769/BioProtoc.3071>.
52. Jayaseelan, S., Doyle, F., and Tenenbaum, S.A. (2014). Profiling post-transcriptionally networked mRNA subsets using RIP-Chip and RIP-Seq. *Methods* 67, 13–19. <https://doi.org/10.1016/j.jymeth.2013.11.001>.
53. Kim, D., Langmead, B., and Salzberg, S.L. (2015). HISAT: a fast spliced aligner with low memory requirements. *Nat. Methods* 12, 357–360. <https://doi.org/10.1038/nmeth.3317>.
54. Anders, S., Pyl, P.T., and Huber, W. (2015). HTSeq—a Python framework to work with high-throughput sequencing data. *Bioinformatics* 31, 166–169. <https://doi.org/10.1093/bioinformatics/btu638>.
55. Love, M.I., Huber, W., and Anders, S. (2014). Moderated estimation of fold change and dispersion for RNA-seq data with DESeq2. *Genome Biol.* 15, 550. <https://doi.org/10.1186/s13059-014-0550-8>.
56. Benjamini, Y., Drai, D., Elmer, G., Kafkafi, N., and Golani, I. (2001). Controlling the false discovery rate in behavior genetics research. *Behav. Brain Res.* 125, 279–284. [https://doi.org/10.1016/s0166-4328\(01\)00297-2](https://doi.org/10.1016/s0166-4328(01)00297-2).
57. Zhang, B., Schmoyer, D., Kirov, S., and Snoddy, J. (2004). GOTree Machine (GOTM): a web-based platform for interpreting sets of interesting genes using Gene Ontology hierarchies. *BMC Bioinf.* 5, 16. <https://doi.org/10.1186/1471-2105-5-16>.
58. Shannon, P., Markiel, A., Ozier, O., Baliga, N.S., Wang, J.T., Ramage, D., Amin, N., Schwikowski, B., and Ideker, T. (2003). Cytoscape: a software environment for integrated models of biomolecular interaction networks. *Genome Res.* 13, 2498–2504. <https://doi.org/10.1101/gr.1239303>.
59. Kraeuter, A.K., Guest, P.C., and Sarnyai, Z. (2019). The open field test for measuring locomotor activity and anxiety-like behavior. *Methods Mol. Biol.* 1916, 99–103. [https://doi.org/10.1007/978-1-4939-8994-2\\_9](https://doi.org/10.1007/978-1-4939-8994-2_9).
60. Kraeuter, A.K., Guest, P.C., and Sarnyai, Z. (2019). The elevated plus maze test for measuring anxiety-like behavior in rodents. *Methods Mol. Biol.* 1916, 69–74. [https://doi.org/10.1007/978-1-4939-8994-2\\_4](https://doi.org/10.1007/978-1-4939-8994-2_4).
61. Can, A., Dao, D.T., Terrillon, C.E., Piantadosi, S.C., Bhat, S., and Gould, T.D. (2011). The tail suspension test. *J. Vis. Exp.* 59, e3769. <https://doi.org/10.3791/3769>.
62. Yankelevitch-Yahav, R., Franko, M., Huly, A., and Doron, R. (2015). The forced swim test as a model of depressive-like behavior. *J. Vis. Exp.* 97, e52587. <https://doi.org/10.3791/52587>.

STAR★METHODS

KEY RESOURCES TABLE

REAGENT or RESOURCE	SOURCE	IDENTIFIER
<i>Antibodies</i>		
Rat anti-BrdU	Abcam	Cat#ab6326; RRID: AB_305426
Rabbit anti-SRSF10	Abcam	Cat#ab254935
Rabbit anti-PAX6	MBL	Cat#PD022; RRID: AB_1520876
Mouse anti-PAX6	Abcam	Cat#ab78545; RRID: AB_1566562
Rat anti-TBR2	e-Bioscience	Cat#14-4875-82; RRID: AB_11042577
Rabbit anti-Ki67	Abcam	Cat#ab15580; RRID: AB_805388
mouse anti-SOX2	CST	Cat#4900; RRID: AB_10560516
goat anti-GFP	Abcam	Cat#ab6673; RRID: AB_305643
rabbit anti-BRN2	CST	Cat#P20265
rabbit anti-TBR1	Abcam	Cat#ab31940; RRID: AB_2200219
rat anti-CTIP2	Abcam	Cat#ab18465; RRID: AB_2064130
mouse anti-Nestin	Millipore	Cat#MAB353; RRID: AB_94911
rabbit anti-CC3	CST	Cat#9664; RRID: AB_2070042
rabbit anti-MAP2	CST	Cat#4542S; RRID: AB_10693782
rabbit anti-NeuN	CST	Cat#24307S; RRID: AB_2651140
rabbit anti-NeuN	Abcam	Cat#ab177487; RRID: AB_2532109
mouse anti-GFAP	Millipore	Cat#MAB360; RRID: AB_11212597
mouse anti-Tuj1	CST	Cat#4466; RRID: AB_1904176
Goat anti Rabbit Alexa Flour 647	Invitrogen	Cat#A21244; RRID: AB_2535812
Goat anti Rat Alexa Flour 568	Invitrogen	Cat#A11077; RRID: AB_2534121
Goat anti Mouse Alexa Flour 555	Invitrogen	Cat#A48287; RRID: AB_2896353
Goat anti Rabbit Alexa Flour 555	CST	Cat#4413; RRID: AB_10694110
Goat anti Mouse Alexa Flour 488	CST	Cat#4408; RRID: AB_10694704
Goat anti mouse Alexa Flour 594	CST	Cat#8890; RRID: AB_2714182
mouse anti-Flag	Abmart	Cat#M20008; RRID: AB_2713960
rabbit anti-SOX2	CST	Cat#23064S; RRID: AB_2714146
rabbit anti-SRSF10	MBL	Cat#RN064PW; RRID: AB_11124967
mouse anti-PCNA	Abcam	Cat#ab29; RRID: AB_303394
mouse anti-β-actin	Sigma	Cat#A5441; RRID: AB_476744
rabbit anti-AKT	CST	Cat#4060; RRID: AB_2315049
rabbit anti-p-AKT	CST	Cat#4691; RRID: AB_915783
rabbit anti-p-mTOR	CST	Cat#2971S; RRID: AB_330970
rabbit anti-NASP	Abcam	Cat#ab181169
Normal Rabbit IgG	CST	Cat#2729S; RRID: AB_1031062
Rabbit anti-SRSF10	ABclonal	Cat#A6024; RRID: AB_2772391
680RD Goat anti-Mouse IgG Secondary Antibody	LI-COR ODYSSEY	Cat#926-68070; RRID: AB_10956588
800CW Goat anti-Mouse IgG Secondary Antibody	LI-COR ODYSSEY	Cat#926-32210; RRID: AB_621842

(Continued on next page)

**Continued**

REAGENT or RESOURCE	SOURCE	IDENTIFIER
680RD Goat anti-Rabbit IgG Secondary Antibody	LI-COR ODYSSEY	Cat#926-68071; RRID: AB_10956166
800CW Goat anti-Rabbit IgG Secondary Antibody	LI-COR ODYSSEY	Cat#926-32211; RRID:AB_621843

Chemicals, peptides, and recombinant proteins

DAPI	Roche	Cat#10236276001
bFGF	Peprotech	Cat#450-33-50
EGF	Peprotech	Cat#315-09-100
B27	Thermo Fisher	Cat#17504044
Accutase	Thermo Fisher	Cat#00-4555-56
GlutaMax	Thermo Fisher	Cat#35050061

Critical commercial assays

BeyoClick™ EdU-647 Cell Proliferation Assay Kit	Beyotime	Cat#C0081
Total RNA Kit I	OMEGA	Cat#R6834-01
Hifair® II 1st Strand cDNA Synthesis SuperMix	YEASEN	Cat#11120ES60
2×TSINGKE® Master qPCR Mix (SYBR Green I)	TSINGKE	Cat#TSE201
HiScript RT SuperMix	Vazyme biotech	Cat#R223-01
Cell Cycle and Apoptosis Assay Kit	Beyotime	Cat#C1052
Immunoprecipitation kit (Protein A+G magnetic beads)	Beyotime	Cat#P2179S

Deposited data

RNA-seq data	This paper	GEO: GSE225647
--------------	------------	----------------

Experimental models: Cell lines

Neuro 2a	ATCC	N/A
----------	------	-----

Experimental models: Organisms/strains

Mouse: ICR	Vital River	N/A
Mouse: C57BL/6	Shanghai Model Organisms and Shanghai SLAC Laboratory Animal Co.,Ltd	N/A
Mouse: Nestin-Cre	Shanghai Research Center for Model Organisms	N/A
Mouse: <i>Srsf10</i> <sup>flox/flox</sup> Nestin-Cre <sup>+</sup>	This paper	N/A

Oligonucleotides

Primer: <i>Srsf10</i> Forward: TAGATGTTTATGTCCCACTTG	This paper	N/A
Primer: <i>Srsf10</i> Reverse: TTTCTAGGACTGTAAGATCTCC	This paper	N/A
Primer: <i>tNasp</i> Forward: TGAAGCATCACCAGTCGTGG	This paper	N/A
Primer: <i>tNasp</i> Reverse: GGCTACCTGGTCTCAACCC	This paper	N/A
Primer: <i>Ccnd2</i> Forward: ACCTCCCGCAGTGTCCCTATT	This paper	N/A
Primer: <i>Ccnd2</i> Reverse: CACAGACTCTAGCATCCAGG	This paper	N/A
Primer: <i>GAPDH</i> Forward: GAACCACGAGAAATATGACAAC	This paper	N/A
Primer: <i>GAPDH</i> Reverse: ATGGCATGGACTGTGGTCA	This paper	N/A
Primer: <i>Nasp</i> Forward: TGAAGCATCACCAGTCGTGG	This paper	N/A
Primer: <i>Nasp</i> Reverse: GGCTACCTGGTCTCAACCC	This paper	N/A
Primer: $\beta$ -actin Forward: CCTCTTGGGTATGGAATC	This paper	N/A
Primer: $\beta$ -actin Reverse: GGAGCAATGATCTTGATC	This paper	N/A
Primer: <i>Bclaf1</i> Forward: CGTTCCAGAACATATTCGAGGTC	This paper	N/A
Primer: <i>Bclaf1</i> Reverse: CCCATAAGGTCGTCTCATTCT	This paper	N/A

(Continued on next page)

**Continued**

REAGENT or RESOURCE	SOURCE	IDENTIFIER
siRNA targeting sequence: SRSF10: GAAGACGCUUUACAUAUUUGGACA	This paper	N/A
shRNA sequence in pSuper-Scramble: CGUUAUCGCGUAUAUACGCGUAU	This paper	N/A
Targeting sequence in LV-shSRSF10: GAAACAGUAGACCGACUGGAA	Heyuan Biotechnology (Shanghai) Co., Ltd	N/A
Targeting sequence in LV-Ctrl: CCUAAGGUUAAGUCGCCUCG	Heyuan Biotechnology (Shanghai) Co., Ltd	N/A
<b>Recombinant DNA</b>		
LV-shSRSF10	Heyuan Biotechnology (Shanghai) Co., Ltd	N/A
LV-Ctrl	Heyuan Biotechnology (Shanghai) Co., Ltd	N/A
Plasmid: pSuper-SRSF10-shRNA	This paper	N/A
Plasmid: pSuper-Scramble	This paper	N/A
Plasmid: pSuper	OligoEngine	Cat#VEC-PBS-0002
Plasmid: pCAG-EGFP	Addgene	Cat#11150
<b>Software and algorithms</b>		
Prism 7	GraphPad Inc.	N/A
NIS-Elements AR	Nikon	N/A
Photoshop CC 2018	Adobe	N/A
CASH	Wu et al. <sup>48</sup>	N/A
Cytoscape	Shannon et al. <sup>58</sup>	N/A

**RESOURCE AVAILABILITY****Lead contact**

Further information and requests for resources, reagents and data should be directed to the lead contact, Dr. Xianhua Chen ([xhchen@fudan.edu.cn](mailto:xhchen@fudan.edu.cn)).

**Materials availability**

Plasmids and mouse lines generated in this study are available from lead contact upon request.

**Data and code availability**

- Data reported in this paper will be shared by the [lead contact](#) upon request.
- The accession number for the RNA sequencing data reported in this paper is GEO: GSE225647 (<https://www.ncbi.nlm.nih.gov/geo/query/acc.cgi?acc=GSE225647>).
- This paper does not report original code.
- Any additional information required to reanalyze the data reported in this paper is available from the [lead contact](#) upon request.

**EXPERIMENTAL MODEL AND STUDY PARTICIPANT DETAILS****Experimental animals**

ICR mice were obtained from Vital River Laboratory Animal Technology Company. For staging of embryos, mid-day of the vaginal plug identified was calculated as embryonic day 0.5 (E0.5). C57BL/6 mice were provided by Shanghai Model Organisms and Shanghai SLAC Laboratory Animal Co., Ltd. All mice were kept in a temperature controlled (25°C) room on a 12/12-h light/dark cycle, with food and water *ad libitum*. For the experiments of embryonic and P0 to P7 mice, both male and female littermates were randomly assigned to experimental groups. For the experiments of 2-month-old mice, males

were used. All animal experiments and surgical procedures were approved by the Institutional Animal Care and Fudan University Shanghai Medical College Committee (IACUC Animal Project 20170223–092), and in strict accordance with the recommendations in the Guide for the care and use of laboratory animals of the National Institutes of Health.

### Generation of SRSF10 conditional knockout mice

The SRSF10 conditional knockout (cKO) mice were generated via the Cre/loxP system. The *Srsf10*<sup>fl<sup>ox</sup></sup> mice we constructed previously<sup>16</sup> were bred with Nestin-Cre mice (generated by Shanghai Research Center for Model Organisms, Shanghai, China) to generate *Srsf10*<sup>fl<sup>ox</sup>/+</sup> Nestin-Cre<sup>+</sup> mice (SRSF10 heterozygous conditional knockout mice, SRSF10 HET cKO mice), which were further bred with *Srsf10*<sup>fl<sup>ox</sup>/fl<sup>ox</sup></sup> mice to generate *Srsf10*<sup>fl<sup>ox</sup>/fl<sup>ox</sup></sup> Nestin-Cre<sup>+</sup> mice (SRSF10 cKO mice). In all the experiments, the *Srsf10*<sup>fl<sup>ox</sup>/fl<sup>ox</sup></sup> mice were used as the control of SRSF10 cKO mice.

### Construction of recombinant pSuper plasmid and lentivirus for SRSF10 knockdown

For SRSF10 knockdown, a previously-validated siRNA sequence of GAAGACGCUUUACAUAUUU GGACA was used as the targeting sequence, and its corresponding short hairpin RNA (shRNA) coding sequence was cloned into the pSuper plasmid between the enzyme sites of BglIII and HindIII. The constructed plasmid was named pSuper-SRSF10-shRNA. The pSuper plasmid containing the shRNA coding sequence of scrambled sequence (CGUUAUCGCGUAUAUACGCGUAU) was used as the negative control (pSuper-Ctrl).

The recombinant lentivirus for mouse SRSF10 knockdown (LV-shSRSF10) and its control (LV-Ctrl) were constructed by Heyuan Biotechnology (Shanghai) Co., Ltd. The targeting sequences in LV-shSRSF10 and LV-Ctrl are listed in the “[key resources table](#)”.

## METHOD DETAILS

### In utero electroporation

*In utero* Electroporation (IUE) was performed according to the reported methods.<sup>49</sup> Timely pregnant mice were anesthetized by isoflurane gas and uterine horns were exposed. Then, recombinant plasmid (final concentration 1.5 μg/μl) mixed with enhanced GFP plasmid (pCAG-EGFP) at a 3:1 mol ratio and 0.1% fast green solution was injected into the lateral ventricle of embryos with glass capillaries. After injection, five square 50 ms pulses of 45 V with 950 ms intervals were applied with an electroporator (BTX, 45–0489). After electroporation, the uterine horns were placed back into the abdominal cavity and the wound was sutured. 2 days or other proper time later, the pregnant mice were sacrificed and the embryonic brains were obtained for a further analysis.

### EdU/BrdU labeling

For cell proliferation analysis in embryonic brains, EdU (5 mg/kg) was injected into pregnant mice via an intraperitoneal (i.p.) injection 2 h before the mice were sacrificed and the embryonic brains were collected for analysis. For the cell-cycle exit experiment, EdU (5 mg/kg) was administered 48 h after utero electroporation, 24 h later, the embryonic brains were collected for further analysis. For the premature NPC terminal mitosis analysis, EdU (5 mg/kg) was administered 24 h after utero electroporation, 3 days later, the embryonic brains were collected for further analysis.

For cell proliferation analysis in the cultured primary NPCs, 10 μM BrdU was added into the culture medium for 1 h before further immunostaining of the BrdU-incorporated cells.

BrdU was immunostained using anti-BrdU antibody (Abcam, ab6326). For BrdU staining, samples need to be treated sequentially in 1N, 2N HCl for 10 minutes at 4°C before permeabilization, followed by 10 minutes of retreatment with boric acid. EdU-incorporated cells was detected by fluorescent dye labeled azide probe, according to the supplier’s protocol (Beyotime, C0081).

### Cell culture

Neural progenitor cells (NPCs) were derived from E14.5 mouse embryonic cerebral cortex according to the reported protocols with a little changes.<sup>50</sup> Briefly, NPCs were cultured in DMEM/F12 medium containing 20 ng/μl bFGF, 20 ng/μl EGF, 5 μg/mL heparin, B27 supplement, GlutaMax, and penicillin/streptomycin.

For neurosphere culture, NPCs were passaged using Accutase (Thermo) every 5 days and planted at  $2 \times 10^5$ /ml. For adherent culture, NPCs were planted on POL/Laminin (Sigma) co-coated slides at  $1.5 \times 10^5$ /ml. All experiments were performed using neurospheres in passage 3-6 and cells from at least 3 individuals. To induce differentiation, adherent NPCs were switched to DMEM/F12 medium containing 2% FBS, 5  $\mu$ g/mL heparin, B27 supplement, glutamine, and penicillin/streptomycin for 5 days. Neuro 2a (N2a), a mouse neural crest-derived cell line from ATCC, was maintained in MEM medium supplemented with 10% FBS. Cells were cultured in a humidified incubator at 37°C with 5%CO<sub>2</sub>.

### Cell transfection and infection

Transfections of pSuper-SRSF10-shRNA plasmid (pSuper-Scramble as the control) were conducted using Lipofectamine 3000 Reagent (Thermo Fisher Scientific) following the supplier's protocol for SRSF10 knock-down. Briefly, cultured N2a cells were transfected with 1  $\mu$ g recombinant plasmid mixed with 0.3  $\mu$ g enhanced GFP plasmid per well of 24-well plate, in the presence of 2.6  $\mu$ l Lipofectamine 3000 Reagent. Cells were transferred to differentiation culture or harvested for further investigation after 48h.

Infections of SRSF10 shRNA-expressing lentivirus or scrambled shRNA-expressing lentivirus (as the control) were performed in primary cultured mouse NPCs. Both lentiviruses express green fluorescent protein. 12 h after cell inoculation, the lentivirus, infection reagents and medium were mixed in a certain ratio and added to the plates by liquid exchange. The MOI of lentivirus infection in this subject was 30. 20-24h after lentivirus infection, the medium containing lentivirus was replaced by fresh lentivirus-free ones. Follow-up experiments were performed 72 h after infections.

### Immunofluorescent labeling of brain sections and cells

Mouse embryonic brains were fixed in 4% PFA solution at 4°C for 8 h and dehydrated in 30% sucrose until they sank to the bottom of the tube. Postnatal and adult brains were fixed in 4% PFA overnight at 4°C and followed by dipping in 20% and 30% sucrose at 4°C successively until the brains were sunk. Brains were then embedded in O.C.T compound (Sakura). Brains were sectioned into 20- $\mu$ m thickness for adult mouse brain and 14- $\mu$ m thickness for embryonic brains or new born mouse brains. Cryosections were permeabilized and incubated with blocking solution (0.1% Triton X-100, 10% normal goat or horse serum in PBS) for 1 h at room temperature. After incubation with the primary antibody at 4°C overnight (for more than 16 h), sections were washed with PBS and incubated with appropriate fluorescence-conjugated secondary antibodies at room temperature for 1 h and counterstained with DAPI before mounting. For immunostainings that need antigen retrieval, slices were kept in citric acid-sodium citrate buffer at 95°C for 10 (embryo) or 20 (adult) minutes before permeabilized.

Immunostaining for cultured cells was performed according to the following procedure: the cells were washed with PBS, fixed in 4% PFA for 30 min at room temperature, permeabilized by 0.2% Triton-100 in PBS. The subsequent operation was the same as the brain sections described above. The primary antibodies and secondary antibodies used in the immunofluorescent labeling for each protein of interest are listed in the "key resources table".

### Western blotting

Tissue or cell lysates (approximately 30–40  $\mu$ g total proteins each) were separated in 12% SDS-PAGE gels and blotted on NC membranes (110v, 1 h). For animal tissue samples, the membranes were blocked with TBST solution containing 5% skim milk at room temperature for 1 h, while for cellular protein samples, the membranes were blocked with high efficiency blocking solution (Willget) at room temperature for 15 min. The membranes were then incubated with primary antibody at 4°C overnight, after that the membranes were washed with TBST for 3 times and incubated with appropriate secondary antibodies at room temperature for 1 h. Signals were detected with an odyssey scanner. The primary antibodies and secondary antibodies used in the Western blot for each protein of interest are listed in the "key resources table".

### RT-PCR

The total RNA of tissue or cells was extracted through Total RNA Kit (OMEGA). Then, the cDNA was generated by using the Hifair® II 1st Strand cDNA Synthesis Kit (YEASEN). RT-qPCR was performed using the SYBR Green kit (TSINGKE) on a LightCycler 96 instrument (Eppendorf). GAPDH was used as reference

gene for normalization. The qPCR primers used for *Srsf10*, *tNasp*, *Ccnd2*, and *GAPDH* are listed in the “[key resources table](#)”.

### RNA-immunoprecipitation (RIP)

RNA-immunoprecipitation was performed according to the reported protocols with some modification.<sup>51,52</sup> In brief, 10<sup>7</sup> NPCs were lysed in 500 $\mu$ l IP lysis buffer (Willget biotech F07 supplied with 200U/ml RNase inhibitor, 1X protease inhibitor and 1mM DTT) on ice for 10 min, then sonicated for three cycles of 10s on /30s off at low intensity. Cell lysate was then centrifuged for 10 min at 15000g, 4°C to remove cell debris. 40 $\mu$ l Protein A+G magnetic beads (Beyotime, P2179S) were washed three times with NT-2 buffer (50 mM Tris pH 7.4, 150 mM NaCl, 1 mM MgCl<sub>2</sub>, 0.05% Nonidet P-40), and then incubated with 5 $\mu$ g normal Rabbit IgG antibody (CST,2729S) or 5 $\mu$ g SRSF10 antibody (ABclonal, A6024) for 2h in rotator at room temperature. After that, beads bound with antibody were washed for four times in NT2 buffer, and resuspended in 800 $\mu$ l NET-2 buffer (1 $\times$  NT-2 buffer supplied with 20 mM EDTA pH 8.0, 1 mM DTT, 200 units/ml RNase inhibitor). Supernatant of NPC cell lysate was then equally added into the two tubes containing beads bound with SRSF10 antibody or IgG, respectively (each 200 $\mu$ l added, totally 1ml in each tube), then 100 $\mu$ l mixture was put aside from each tube as the input, with the beads removed immediately by magnet. The mixture of cell lysate-antibody bound beads were incubated on rotator at 4°C overnight, followed by a five times washes of the beads using ice cold NT-2. Before the last washing, 1/10 beads were removed for Western Blot analysis. Beads were eventually resuspended in 200 $\mu$ l proteinase K buffer (NT-2 buffer with 1% SDS and 1.2mg/ml proteinase K), and the input was directly added with SDS and proteinase K to the same volume. All tubes were incubated at 55°C for 30 min and inverted every 5 min. RNA was extracted using a Total RNA Kit (Omega, R6834), and reverse transcription were followed using HiScript RT SuperMix (Vazyme biotech, R223-01) to generate cDNA for qPCR. qPCR analysis was then performed as described above. The qPCR primers for *Nasp*,  $\beta$ -actin (as a negative control), and *Bclaf1* (a reported target gene of SRSF10, as a positive control) are listed in the “[key resources table](#)”.

### Cell cycle analysis

Cells were dispersed and fixed with 100% ethanol before being stained with fluorescent dye PI and analyzed by flow cytometry, as described by the supplier’s protocol (Beyotime, C1052). The amount of DNA in each cell was analyzed for determining the phase of cell cycle that the cells located.

### RNA sequencing and bioinformatic analysis

RNA was extracted from dissected P0 cortex of SRSF10 cKO mice and SRSF10 knockdown primary NPCs and their respective controls. For mRNA preparation, total RNA was isolated using TRIzol reagent (Invitrogen, Carlsbad, CA). The RNA quality was checked by Agilent 2200. The qualified RNA for each sample with RIN (RNA integrity number) > 7.0 was constructed into cDNA library using the TruSeq Stranded mRNA Library Prep Kit (Illumina Inc.) according to the manufacturer’s instructions. The libraries were quality controlled with Agilent 2200 and sequenced by NovaSeq 6000 on a 150 bp paired-end run. The clean reads were then aligned to mouse genome (mm10, Ensemble: version 100) using the Hisat2.<sup>53</sup> HTseq<sup>54</sup> was used to get gene counts and RPKM method was used to determine the gene expression. Then, DESeq2 algorithm was applied<sup>55</sup> to filter the differentially expressed genes, after the significant analysis, P-value and FDR analysis<sup>56</sup> were subjected to the following criteria of Fold Change>1.5 or < 0.67, and FDR<0.05. For Gene ontology (GO) analysis, GO annotations from NCBI (<http://www.ncbi.nlm.nih.gov/>), UniProt (<http://www.uniprot.org/>) and the Gene Ontology (<http://www.geneontology.org/>) were downloaded. Fisher’s exact test was applied to identify the significant GO categories (P-value < 0.05). Pathway analysis was performed find out the significant pathway of the differentially expressed genes according to KEGG database. The Fisher’s exact test was applied to select the significant pathway, and the threshold of significance was defined by P-value< 0.05. For construction of GO-Tree, the significant GO-Term (P-Value<0.01) in GO Analysis were selected based on the up and down differentially expressed genes to summarize the function affected by SRSF10 gene knockout/knockdown.<sup>57</sup> For construction of Path-Act-Network, which includes metabolism, membrane transport, signal transduction and cell cycle pathways, the genes in enriched biological pathway were picked and Cytoscape<sup>58</sup> was used for graphical representations of pathways. For the alternative splicing detection, the CASH software<sup>48</sup> were selected as the tool to detect the differentially alternative splicing cases based on the bam file after mapping according to the FDR threshold (FDR<0.05).

### Behavioral testing

Y-maze test, rotarod test, open-field test, elevated plus-maze test, tail suspension test and forced swimming test were analyzed as follows:

Y-maze test was used to evaluate spontaneous alternation as a measure of working memory. This test was performed in a Y-shaped maze with three opaque arms at a 120° angle from each other. The number and order of mice entering the three opaque arms within 10 minutes were recorded using the movement track tracking system of EthoVision software. Over the course of several arm entries, healthy mice should show a tendency to enter a less recently visited arm thus displaying a higher alternation percentage. The mouse entered for three consecutive times into different entries was counted as an alteration. The parameter of alternation behavior was counted as the ratio of the number of alterations / (total arm-entering times-2).

Rotarod task was used to evaluate motor coordination after repeat learning. The ENV-575M Rotarod machine (Med Associates Corp.) was used for this test. For each trial, mice were placed on the rotarod moving at a constant speed of 20 rpm over the course of 5 min, which will fall onto the platform below when they could not coordinate its movement on the rotating rotarod. The latency time to fall from the rotarod was automatically recorded by the software. Every mouse was tested for three consecutive trials a day with 10-min intervals between each trial. And this test was repeated for three consecutive days. The average latency time to fall from the rotating rotarod for the third trial in the test of each day were used for data analysis.

Anxiety and exploratory behaviors were assessed by Open field test. The test was performed according to the reported methods with minor modification.<sup>59</sup> In this test, each animal was placed individually at the border of MED-VOF-MS square arena of Media Associates, which is subdivided into central and conner zone using the EthoVision software tracking system. The movement track of mice in the box within 10 minutes was collected through the induction system. The activity of the mice including the total movement distance, total time spent in the center, and number of central area entries were analyzed.

The elevated plus maze test was used to measure anxiety-like behavior and was performed according to the reported methods.<sup>60</sup> The MED-VPM-MS elevated plus-maze (Med Associates Corp.) was used for this test. The intersection position of the open arm and the closed arm of the elevated maze was set as the central area. The test was initiated by placing the mouse on the central area of the maze, facing one of the open arms, and letting it move freely. Mouse behavior within 5 minutes of being put into the maze was continuously recorded by the software EthoVision, and the data including the movement track, the times entering the open arm, and the duration staying in the open arm were collected by the software.

Tail suspension test was used for evaluating depression-related behaviors and was performed according to the reported methods.<sup>61</sup> The MED-VPM-MS cabinet (Med Associates Corp.) was used for this test. The mice were suspended by their tails with tape, in such a position that it cannot escape or hold on to nearby surfaces. The behavior of the mice was recorded immediately with the photography system, and the duration that the mice staying motionless within the last 4 minutes of a total 6 minutes was counted.

The forced swim test was used for evaluation of depressive-like states and was performed according to the reported methods with minor modification.<sup>62</sup> In this test, a transparent cylindrical container containing water about 10 cm depth was used. The water temperature was kept at 25–30°C. The mice were put into the container and the behavior of the mice was immediately recorded with the photography system. The accumulated time of that the mice staying motionless within the last 4 minutes of a total 6 minutes was counted.

### Confocal imaging

All images were captured with confocal microscopy (Nikon A1R) and analyzed with NIS-Elements AR (Nikon) or Photoshop CC 2018 (Adobe).

### QUANTIFICATION AND STATISTICAL ANALYSIS

All comparisons between the two groups of data were performed using the Two-tailed Student's t-test for independent samples, expressed as mean  $\pm$  standard error (S.E.M.), and statistical data were counted and

plotted using GraphPad Prism 7 software.  $P < 0.05$  was considered statistically significant. Significance is marked as \* $p < 0.05$ , \*\* $p < 0.01$ , \*\*\* $p < 0.001$ , and \*\*\*\* $P < 0.0001$ .

#### **Data and software availability**

The data of RNA-seq discussed in this paper have been deposited into NCBI's Gene Expression Omnibus, and are accessible through GEO Series accession number GSE225647 (<https://www.ncbi.nlm.nih.gov/geo/query/acc.cgi?acc=GSE225647>).